Available online at www.sciencedirect.com
ScienceDirect
Lithos 101 (2008) 359–378
LITHOS
www.elsevier.com/locate/lithos

The Grader layered intrusion (Havre-Saint-Pierre Anorthosite, Quebec) and genesis of nelsonite and other Fe–Ti–P ores

Bernard Charlier [a,*], Emmanuel Sakoma [b], Martin Sauvé [b], Kerry Stanaway [b], Jacqueline Vander Auwera [a], Jean-Clair Duchesne [a]

[a] *Department of Geology, B20, University of Liège, 4000 Sart Tilman, Belgium*
[b] *Rio Tinto Iron & Titanium Inc., Canada*

Received 16 October 2006; accepted 6 August 2007
Available online 16 August 2007

Abstract

The Grader layered intrusion is part of the Havre-Saint-Pierre anorthosite in the Grenville Province (Quebec, Canada). This intrusion has a basin-like morphology and contains significant resources of Fe–Ti–P in ilmenite and apatite. Outcropping lithologies are massive oxide alternating with anorthosite layers, banded ilmenite–apatite–plagioclase rocks and layered oxide apatite (gabbro-)norites. Drill cores provide evidence for stratigraphic variations of mineral and whole rock compositions controlled by fractional crystallization with the successive appearance of liquidus phases: plagioclase and ilmenite followed by apatite, then orthopyroxene together with magnetite, and finally clinopyroxene. This atypical sequence of crystallization resulted in the formation of plagioclase–ilmenite–apatite cumulates or "nelsonites" in plagioclase-free layers. Fine-grained ferrodiorites that cross-cut the cumulates are shown to be in equilibrium with the noritic rocks. The high TiO_2 and P_2O_5 contents of these assumed liquids explains the early saturation of ilmenite and apatite before Fe–Mg silicates, thus the nelsonites represent cumulates rather than crystallized Fe–Ti–P-rich immiscible melts. The location of the most evolved mineral and whole rock compositions several tens of meters below the top of the intrusion, forming a sandwich horizon, is consistent with crystallization both from the base and top of the intrusion. The concentrations of V and Cr in ilmenite display a single fractionation path for the different cumulus assemblages and define the cotectic proportion of ilmenite to 21 wt.%. This corresponds to bulk cotectic cumulates with ca. 8 wt.% TiO_2, which is significantly lower than what is commonly observed in the explored portion of the Grader intrusion. The proposed mechanism of ilmenite-enrichment is the lateral removal of plagioclase due to its relative buoyancy in the dense ferrodiorite melt. This plagioclase has probably accumulated in other portions of the intrusion or has not been distinguished from the host anorthosite.

Keywords: Anorthosite; Grenville; Fe–Ti deposit; Ilmenite; Layered intrusion; Nelsonite

1. Introduction

Despite the discovery of the Voisey's Bay Ni–Cu deposits in Proterozoic Anorthosite–Mangerite–Charnockite–(rapakivi) Granite (AMCG) suites (e.g. Kerr and Ryan, 2000), Fe–Ti oxide deposits remain the major

* Corresponding author. Tel.: +32 4 3662250; fax: +32 4 3662921.
E-mail address: b.charlier@ulg.ac.be (B. Charlier).

0024-4937/$ - see front matter © 2007 Elsevier B.V. All rights reserved.
doi:10.1016/j.lithos.2007.08.004

mineralization type in Proterozoic anorthosite. Two world-class Fe–Ti oxide deposits are currently being mined in massif-type anorthosites: the Tio Mine (Havre-Saint-Pierre anorthosite, Quebec) and the Tellnes deposit (Rogaland anorthosite Province, Norway). At the present time, exploration for ilmenite deposits is not only focused on the grade of the ore but also on finding minerals suitable for industrial processing (e.g. Cr- and Mg-poor ilmenite). A genetic model for the formation of Fe–Ti oxide deposits in massif-type anorthosites is thus crucial for the prediction of the chemical variability of different ore types. Immiscibility of a Fe–Ti–P-rich melt has been invoked for the formation of some ilmenite ore types (e.g. Kolker, 1982; Force, 1991), but more recent studies on the Tellnes ilmenite deposit (Charlier et al., 2006, 2007) have emphasized the role of fractional crystallization with ilmenite as an early liquidus phase.

Layered intrusions are commonly present in anorthositic provinces and several have been studied in detail, including the Kiglapait intrusion of the Nain Plutonic suite (Canada) (e.g. Morse, 1996) and the Bjerkreim–Sokndal layered intrusion in the Rogaland Anorthosite Province (SW Norway; e.g. Wilson et al., 1996). Other intrusions of note include the Newark Island layered intrusion in Labrador (Wiebe and Snyder, 1993) and the Fedorivka layered intrusion in Ukraine (Duchesne et al., 2006). Many other less-studied small intrusions have also intruded anorthosite plutons (e.g. Vander Auwera et al., 2006). These intrusions are commonly interpreted as resulting from the fractional crystallization of anorthosite residual magma to produce a series of cumulate rocks.

The Grader layered intrusion is part of the large Havre-Saint-Pierre anorthosite complex in Quebec, Canada (Hargraves, 1962). The abundance of ilmenite in the Grader intrusion is high, well over 10 vol.%, and much of it has less Cr and Mg than ilmenite that is being mined from the Tio Mine (Bergeron, 1986) and the Tellnes ilmenite deposit (Charlier et al., 2007). The base of the intrusion however contains ilmenite with Cr and Mg contents similar to those of the Tio Mine oxide ore. An exploration campaign on the Grader intrusion yielded complete cores from 10 diamond drill holes. Information from these cores is used to define the structure and to examine the genetic link between the different rock types. Economic resources start at the base with massive ilmenite, then layers of ilmenite alternating with anorthositic layers followed upward by ilmenite–apatite ore (nelsonites) with variable proportions of plagioclase, culminating with oxide apatite (gabbro-)norites. In this paper, the proposed mechanism of ilmenite enrichment in the Grader layered intrusion and the relation between the ore and fine-grained ferrodiorites is considered to be applicable to the formation of Fe–Ti oxide ores in massif-types anorthosites in general, and specifically to the origin of nelsonites.

2. Geological setting

The Grader layered intrusion outcrops in the Allard lobe of the Havre-Saint-Pierre anorthosite complex (Quebec, Canada), which is part of the allochthonous polycyclic belt of the Grenville Province (Rivers et al., 1989). This anorthosite complex is composed of several anorthositic lobes separated by monzonitic, mangeritic to charnockitic envelopes (Fig. 1). The small Rivière au Tonnerre anorthosite was dated at 1062±4 Ma (U–Pb zircon; van Breemen and Higgins, 1993) and a monzonite from the Magpie river area gives an age of 1126^{+7}_{-6} Ma (U–Pb zircon; Emslie and Hunt, 1990; see approximate sample locations on Fig. 1).

The Grader intrusion is located about 4 km southwest of the Tio Mine and contains the Grader mine which was exploited in the late 1940s. A simplified geological map of the intrusion (Fig. 2) shows that the Grader mine was excavated in massive ilmenite containing minor anorthosite. In 2002, ten holes ranging from 75 to 274 m deep were drilled by Rio Tinto Iron & Titanium west of the Grader mine (Fig. 2). These vertical drill holes show that rock contacts (i.e. layers) dips from 0 to 45°. This, combined with surface sampling, ground gravity data and an electro-magnetic survey, allow for a description of the morphology of the Grader intrusion. All results indicate a basin-like structure, with outcropping oxide apatite (gabbro-)norite, banded nelsonite and massive oxide in the north and east that dip southward in the north, westward in the east and steeply north-eastward in the southwest (Fig. 2). This structure is interrupted by faults with NNE–SSW or NE–SW trends. The location of these faults is inferred from drill hole correlations, coupled with the outcrop pattern and orientation of the norite and banded layers; it is also corroborated by gravity interpretation and topographic breaks. These faults displace the east-side blocks upward, except for the NE–SW fault that displaces the east-side downward. The exact location and displacement along these faults are problematic because none were intersected in the drill cores or observed on the limited outcrops. Local variations in dip and strike may be explained by *m*-scale slump-style folds that are prominent in large outcrops of alternating anorthosite and ilmenitite or nelsonite immediately west of the Grader mine. Thin, fine-grained, ferrodiorites dykes with thickness ranging

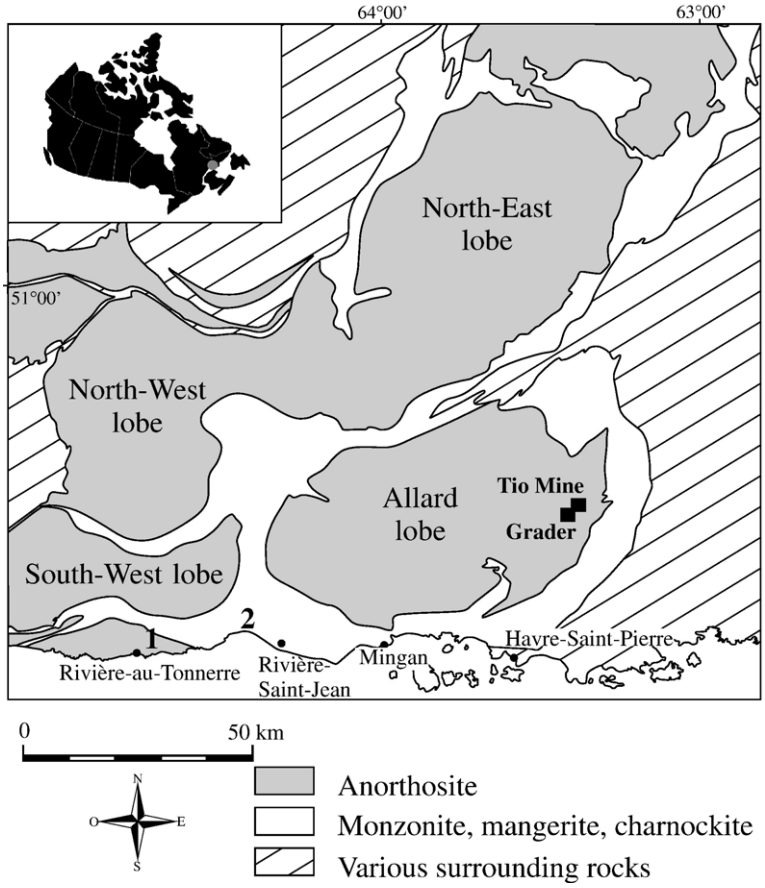

Fig. 1. Simplified geological map of the Havre-Saint-Pierre anorthosite complex in the Grenville Province, Quebec (after Wodicka et al., 2003) showing the location of the Tio Mine and the Grader layered intrusion. Numbers 1 and 2 are the locations of samples with reported U–Pb geochronology, in the Rivière au Tonnerre anorthosite and Magpie monzonite respectively.

from 10 to 30 cm and sharp contacts, locally cross-cut the Grader layered intrusion.

3. Sampling and analytical methods

Twenty-four samples from hole GRD02-03 and from the host Havre-Saint-Pierre pluton were selected for plagioclase separation (60–150 μm) using flotation in bromoform and magnetic separation. Final purification was carried out by HCl leaching to dissolve any composite grains with apatite. Samples ground in agate mortar were analysed for major elements by XRF on Li-borate fused glass and for Sr and Ba by XRF on pressed powder pellets. Ilmenite and magnetite from samples in hole GRD02-03 were separated with heavy liquids (bromoform and Clerici's solution) and magnetic separation, and analysed for major elements (Si, Ti, Al, Fe, Mn, Mg) by XRF on Li-borate fused glass, and for trace elements (ilmenite: Ni, V, Cr, Zn, Zr, Nb; magnetite: Ni, V, Cr, Zn, Mn) on pressed powder pellets. International Fe–Ti oxide reference materials (SARM 59 and 12, IGS 31 and 32, GBW 07226), samples 16716 G/91, V4-1, 16717 provided by Titania A/S, as well as synthetic and in-house standards, measured by other methods, were used for calibration. Apatite was also separated from 8 samples of nelsonite and oxide apatite norite in GRD02-03. Mn, Sr, Y and REE in apatite were determined by ICP-MS. Six fine-grained samples from dykes were analysed for major and trace elements by XRF and ICP-MS. All these analyses were carried out at the Université de Liège (XRF is an ARL 9400 XP and ICP-MS is a VG Plasma Quad PQ2 of Fisons Instruments). Methods for ICP-MS analyses are detailed in Vander Auwera et al. (1998a).

Microprobe analyses of ortho- and clinopyroxene were performed using the JEOL 8900 Series Superprobe of McGill University (Quebec, Canada). An accelerating voltage of 15 kV and a beam current of 15 nA were used. A set of synthetic and natural standards were used: TiO_2 (Ti), magnetite (Fe), spessartine (Mn), olivine (Mg), albite

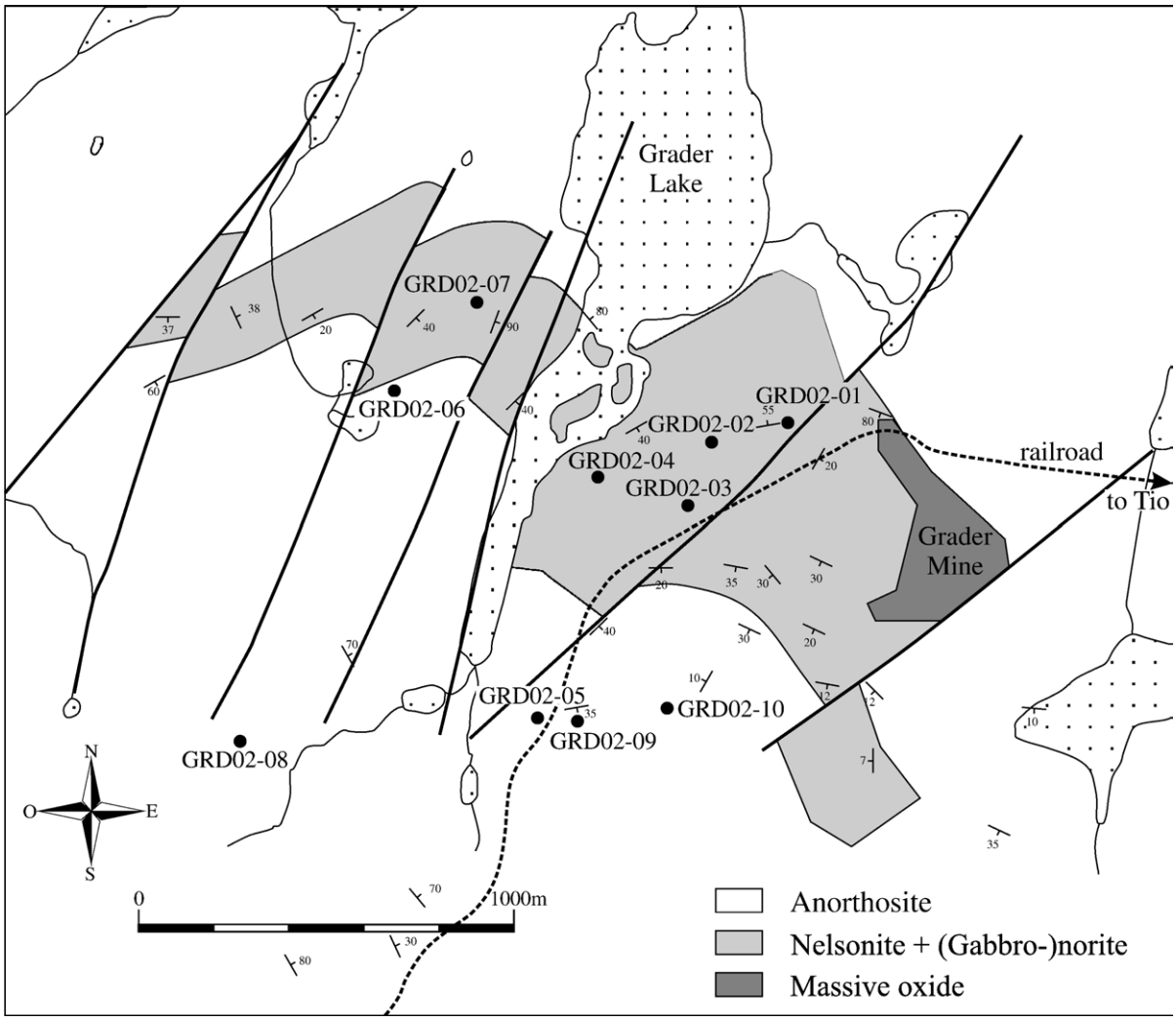

Fig. 2. Simplified geological map of the Grader layered intrusion in the Allard lobe anorthosite showing the locations of drill holes, major faults and orientations of layering.

(Na), orthoclase (K and Al), and diopside (Ca and Si). Chemical analyses were corrected with the ZAF software.

Whole rock samples (259 samples from 10 drill cores) from the Grader intrusion were analysed for major elements by XRF on Li-borate fused glass at SGS Laboratories at Lakefield, Ontario. Each sample represents a 2 m portion of a split drill core taken at approximately 8 m intervals, resulting in a sample every 10 m. The thick 10–50 m intervals of rock described below as banded or layered oxides and nelsonites were sampled at smaller intervals varying between 1 and 6 m. A total of 470 m, corresponding to 25% out of a total 1847 m drilled, was thus analysed by standard methods for bulk composition.

Sr isotopic compositions were measured for 10 plagioclase samples at the Pacific Centre for Isotopic and Geochemical Research, University of British Columbia, on a Thermo Finnigan TRITON-TI mass spectrometer. Prior to separation on ion exchange resin, plagioclase separates were dissolved in a mixture of HF, HNO_3 and $HClO_4$. During the period of measurements, $^{87}Sr/^{86}Sr$ for the NBS 897 Sr standard, normalized to $^{86}Sr/^{88}Sr = 0.1194$, was 0.710237 ± 0.000004 (reference value 0.710240).

4. Results

4.1. Mineralogy and cumulate stratigraphy

The presence of igneous layering in the Grader intrusion is consistent with a cumulate origin for the rocks. The nomenclature of Irvine (1982) is thus applied and rocks are named using the first letter of their cumulus phases followed by -C meaning “cumulus”.

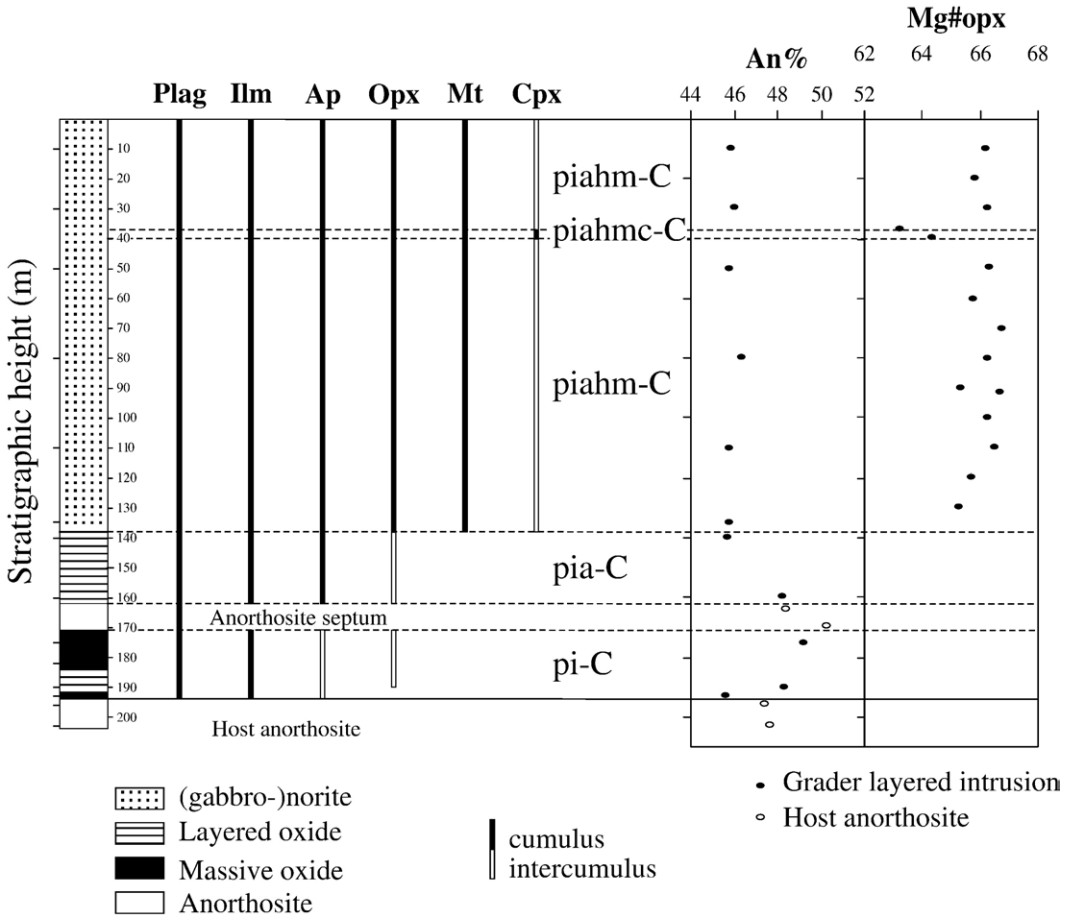

Fig. 3. Cumulate stratigraphy of the Grader layered intrusion and cryptic layering of anorthite (An=100 [Ca/(Ca+Na)]) in plagioclase and Mg# (=100 [Mg/(Mg+Fe)]) of orthopyroxene. Cumulus assemblages following the nomenclature of Irvine (1982). Mineral abbreviations: p = plagioclase; i = ilmenite; a = apatite; h = orthopyroxene; mt = magnetite; c = clinopyroxene; -C = cumulus.

The stratigraphy of the Grader intrusion is displayed in Fig. 3, using observations and mineral compositions from hole GRD02-03. This hole represents the longest section through the intrusion and, as discussed later based on whole rock compositions, is representative of all rock types in the Grader intrusion.

The base of the intrusion starts with a thin sequence of massive oxides (ca. 2 m), followed by 7 m of alternating massive oxide–anorthosite layers. Plagioclase (p) and ilmenite (i) are the main minerals in this cumulate portion (pi-C) (Fig. 4A–B). Small amounts of intercumulus orthopyroxene (2–3 vol.%) may also be present. This is followed by a 12 m massive oxide layer and then by 9 m of anorthosite which may represent an anorthosite septum or a thicker anorthosite layer within the banded unit as discussed later. Above 162 m deep, the cumulates are characterized by the appearance of abundant apatite (a). These pia-C may be referred to as nelsonites (Fig. 4C), a name initially introduced by Watson and Taber (1910) for rutile–apatite and (hemo-)ilmenite–(Ti-)magnetite–apatite rocks. However, most Grader nelsonites contain significant amounts of plagioclase (from 5 to 30 vol.%) and are interlayered with plagioclase-rich rocks (Fig. 4D). The appearance of significant orthopyroxene (h) at 139 m together with magnetite (m) marks the beginning of a ca. 100 m sequence of norites (piahm-C) (Fig. 4E–F). Clinopyroxene (c), commonly present as a minor intercumulus phase, displays a significant increase in modal abundance between 40 and 37 m deep, which indicates a change to a cumulus status. These rocks must thus be referred to as gabbronorite (piahmc-C). Above 37 m, and extending up to the upper contact with the host anorthosite, clinopyroxene returns to an intercumulus status, which results in a sequence of rocks similar in composition to the 100 m-thick sequence of

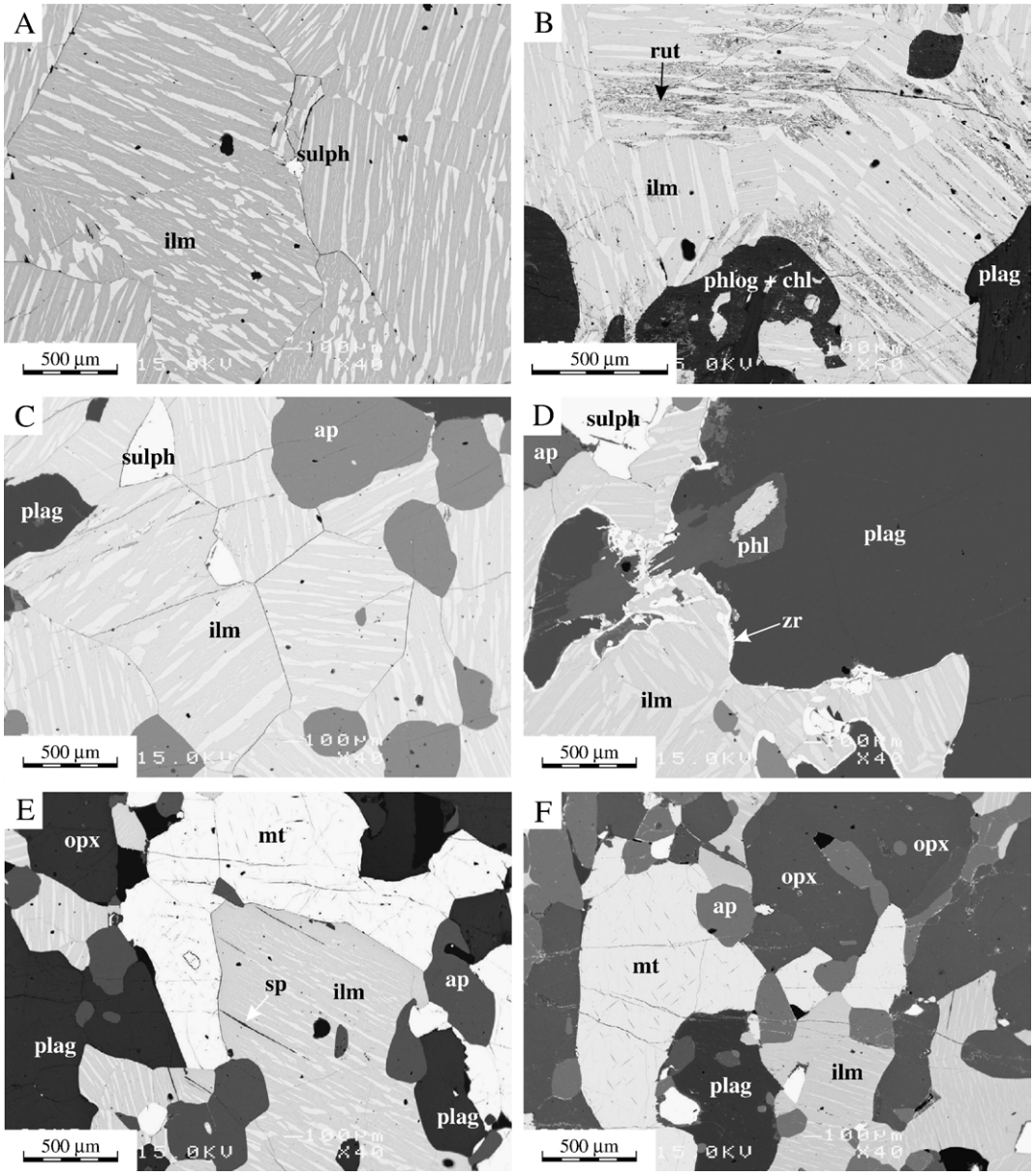

Fig. 4. Backscattered electron (BSE) images of polished thin sections showing petrographic characteristics of the Grader layered intrusion. Minerals were identified with energy dispersive X-ray spectrometry. (A) Massive oxide (GRD02-03 at 180 m) showing hemo-ilmenite with two generations of hematite exsolution lamellae and a small interstitial grain of sulphide. (B) Massive oxide GRD02-03 at 190 m with hemo-ilmenite locally altered to rutile+hematite. (C) Nelsonite (pia-C) (GRD02-03 at 143 m) with large apatite grains, locally included in hemo-ilmenite. (D) Plagioclase-rich nelsonite pia-C (GRD02-03 at 147.5 m). Note hemo-ilmenite continuously rimmed by zircon. (E–F) Norites (piahm-C; GRD02-03 at 130 m and at 10 m). Thin dark aluminous spinel exsolution lamellae (sp) are visible in magnetite and in hemo-ilmenite. A rim depleted in hematite exsolution is observed in the hemo-ilmenite close to the contact with magnetite.

norites (piahm-C) below the gabbronorites. Norites and gabbronorites are texturally more homogeneous than the highly layered base of the intrusion, but may locally display layering characterized by sharply bounded and graded intervals of variable modal proportions at a dm scale.

Accessory minerals in the Grader intrusion mainly include sulphides (pyrite, pyrrhotite and chalcopyrite), Ti-phlogopite and aluminous spinel (hercynite). Zircon commonly rims hemo-ilmenite (Fig. 4D) and traces of baddeleyite are documented. In some massive oxide and altered anorthosite samples, hemo-ilmenite grains may be

Table 1
Major and trace element compositions of separated plagioclase from the Grader layered intrusion and the host Havre-Saint-Pierre (HSP) anorthosite (XRF analyses)

	Rock type	SiO_2	TiO_2	Al_2O_3	Fe_2O_{3tot}	MgO	CaO	Na_2O	K_2O	Total	An	Or	Ba	Sr
HSP-AN-01	HSP anorthosite	56.51	0.06	26.54	0.21	0.01	9.43	5.50	0.66	98.90	48.6	3.9	264	1223
HSP-AN-02	HSP anorthosite	57.31	0.02	26.13	0.67	0.12	8.69	5.58	0.71	99.22	46.3	4.3	225	1143
HSP-AN-03	HSP anorthosite	56.92	0.03	27.52	0.13	0.03	9.35	5.58	0.70	100.27	48.1	4.1	212	1202
HSP-AN-04	HSP anorthosite	57.31	0.03	27.25	0.06	0.03	9.09	5.62	0.90	100.28	47.2	5.3	244	1194
GRD02-06 at 4 m	Roof anorthosite	58.84	0.04	25.97	0.29	0.09	7.97	5.26	1.15	99.60	45.5	7.2	331	1108
GRD02-05 at 10 m	Roof anorthosite	56.41	0.05	27.06	0.21	0.06	9.60	5.26	0.76	99.42	50.2	4.5	247	1209
GRD02-08 at 60 m	Roof anorthosite	58.06	0.04	26.24	0.14	0.04	8.54	5.58	1.10	99.73	45.8	6.6	439	1168
GRD02-10 at 4 m	Roof anorthosite	57.80	0.05	26.24	0.30	0.05	8.71	5.49	1.09	99.73	46.7	6.5	519	1139
GRD02-07 at 130 m	Roof anorthosite	57.22	0.03	26.41	0.15	0.04	8.82	5.65	0.93	99.24	46.3	5.5	255	1209
GRD02-03 at 196 m	Floor anorthosite	57.32	0.03	26.82	0.09	0.01	9.31	5.71	0.69	99.98	47.4	4.0	243	1209
GRD02-03 at 203 m	Floor anorthosite	57.30	0.03	26.62	0.08	0.01	9.34	5.66	0.68	99.73	47.7	4.0	221	1231
GRD02-03 at 164 m	Anorthosite septum	57.74	0.03	26.81	0.14	0.01	9.27	5.46	0.98	100.44	48.4	5.7	439	1128
GRD02-03 at 170 m	Anorthosite septum	55.83	0.04	26.59	0.13	0.01	9.73	5.31	0.66	98.31	50.3	3.9	213	1156
GRD02-03 at 10 m	Norite (piahm-C)	57.54	0.04	26.38	0.06	0.02	8.74	5.70	0.91	99.39	45.8	5.4	469	1315
GRD02-03 at 30 m	Norite (piahm-C)	57.44	0.04	26.17	0.15	0.02	8.73	5.70	1.02	99.26	45.8	6.0	534	1311
GRD02-03 at 50 m	Norite (piahm-C)	57.93	0.05	26.08	0.17	0.01	8.69	5.68	1.08	99.69	45.8	6.4	502	1297
GRD02-03 at 80 m	Norite (piahm-C)	57.87	0.04	26.49	0.20	0.01	8.77	5.60	1.08	100.06	46.4	6.4	594	1282
GRD02-03 at 110 m	Norite (piahm-C)	58.02	0.04	26.13	0.15	0.01	8.78	5.74	0.99	99.87	45.8	5.8	500	1307
GRD02-03 at 135 m	Norite (piahm-C)	57.90	0.04	26.32	0.10	0.01	8.83	5.71	0.99	99.90	46.1	5.8	505	1331
GRD02-03 at 140 m	Nelsonite (pia-C)	58.03	0.04	26.27	0.14	0.01	8.39	5.50	1.20	99.59	45.7	7.2	557	1341
GRD02-03 at 160 m	Nelsonite (pia-C)	55.63	0.03	26.11	0.08	0.01	9.26	5.49	0.59	97.21	48.3	3.5	306	1335
GRD02-03 at 175 m	Massive oxide (pi-C)	55.56	0.06	26.95	0.07	0.14	9.82	5.60	0.14	98.35	49.2	0.8	–	–
GRD02-03 at 190 m	Massive oxide (pi-C)	56.43	0.05	27.05	0.12	0.04	9.43	5.58	0.74	99.44	48.3	4.3	305	1210
GRD02-03 at 193 m	Massive oxide (pi-C)	57.22	0.04	26.91	0.53	0.08	8.87	5.84	0.53	100.03	45.6	3.2	260	1153

An = 100 [Ca/(Ca+Na)]; Or = 100 [K/(Ca+Na+K)]; Sr and Ba in ppm.

locally strongly altered and replaced by rutile+hematite± titanite (Fig. 4B).

The host anorthosite in direct contact with massive oxide at the base of the Grader intrusion is incipiently altered to sericite and epidote. Below this contact zone, the anorthosite is massive and heterogranular with grain-size ranging from 0.1 mm to >2 cm. This is interpreted as a result of dynamic recrystallization (i.e. primary crystals are replaced by smaller recrystallized grains). The anorthosite is typically pure plagioclase but may contain minor amounts of ilmenite, orthopyroxene, apatite and sulphides. The anorthosite at the roof of the

Table 2
Microprobe analyses of orthopyroxene in hole GRD02-03 in the Grader layered intrusion

Depth (m)		SiO_2	TiO_2	Al_2O_3	FeO	MnO	MgO	CaO	Total	Mg #
10	piahm-C	52.33	0.08	1.83	21.26	0.60	23.40	0.56	100.06	66.2
20	piahm-C	52.24	0.12	1.87	21.53	0.58	23.28	0.64	100.26	65.8
30	piahm-C	52.24	0.13	1.87	21.10	0.59	23.23	0.73	99.89	66.2
37	piahmc-C	52.49	0.10	1.54	22.96	0.62	22.17	0.82	100.69	63.2
40	piahmc-C	52.45	0.13	1.57	22.44	0.59	22.70	0.72	100.59	64.3
50	piahm-C	52.26	0.10	1.88	21.35	0.61	23.61	0.67	100.47	66.3
60.5	piahm-C	52.38	0.12	2.03	21.43	0.55	23.12	0.66	100.29	65.8
70	piahm-C	52.49	0.11	1.91	20.68	0.56	23.28	1.27	100.29	66.7
80	piahm-C	52.23	0.09	1.99	21.34	0.57	23.53	0.60	100.34	66.3
90	piahm-C	52.22	0.16	2.02	21.71	0.56	22.94	0.80	100.40	65.3
91.85	piahm-C	52.11	0.12	2.10	20.91	0.52	23.50	0.59	99.84	66.7
100	piahm-C	52.45	0.09	1.93	21.20	0.56	23.38	0.60	100.20	66.3
110	piahm-C	51.72	0.10	1.79	20.97	0.53	23.34	0.76	99.22	66.5
120	piahm-C	51.68	0.12	1.89	21.54	0.55	23.13	0.73	99.64	65.7
130	piahm-C	51.34	0.14	1.97	21.82	0.60	23.03	0.67	99.56	65.3

Mg# = 100 [Mg/(Mg+Fe)].

Table 3
Microprobe analyses of clinopyroxene in hole GRD02-03 in the Grader layered intrusion

Depth (m)		SiO_2	TiO_2	Al_2O_3	FeO	MnO	MgO	CaO	Na_2O	Total	Mg #	En	Fs	Wo
10	piahm-C	51.00	0.49	3.26	9.98	0.30	13.59	21.39	0.59	100.60	70.8	39.3	16.2	44.5
20	piahm-C	50.73	0.41	3.01	10.02	0.24	13.90	20.72	0.52	99.55	71.2	40.4	16.3	43.3
37	piahmc-C	51.43	0.42	2.62	9.77	0.30	13.33	22.25	0.52	100.63	70.9	38.3	15.7	46.0
40	piahmc-C	50.53	0.49	3.12	10.15	0.28	12.80	21.84	0.62	99.83	69.2	37.4	16.7	45.9
50	piahm-C	51.28	0.55	3.41	8.72	0.28	13.49	22.79	0.58	101.10	73.4	38.8	14.1	47.1
60.5	piahm-C	51.22	0.38	2.92	8.96	0.27	14.09	22.31	0.49	100.63	73.7	40.1	14.3	45.6

Mg#=100 [Mg/(Mg+Fe)]; En=100 [Mg/(Mg+Fe+Ca)]; Fs=100 [Fe/(Mg+Fe+Ca)]; Wo=100 [Ca/(Mg+Fe+Ca)].

intrusion was intersected in several drill cores and is similar to that at the base. The anorthosite layer between 172 and 161 m (Fig. 3) displays petrographic features similar to the host anorthosite.

4.2. Mineral chemistry

4.2.1. Plagioclase

The range of plagioclase compositions in the Grader intrusion and in the surrounding Allard lobe anorthosite is highly restricted (Table 1). Bulk plagioclase compositions in the Grader intrusion vary from $An_{49.2}$ to $An_{45.6}$ (An=100 [Ca/Ca+Na]) and $Or_{0.8}$ to $Or_{7.2}$ (Or=100 [K/Ca+Na+K]). Sr contents vary from 1153 to 1335 ppm and Ba contents from 260 to 594 ppm. These compositions are similar to the range of plagioclase compositions in the Havre-Saint-Pierre anorthosite: $An_{50.3–45.5}$, $Or_{3.9–7.2}$, Sr=1108–1231 ppm and Ba=212–519 ppm. Plagioclase compositions in the anorthosite septum ($An_{48.4–50.3}$, Ba=213–439 ppm, Sr=1128–1156 ppm) are similar to those from the base of the Grader intrusion and also to plagioclase of the host Allard lobe anorthosite. The stratigraphic variation of plagioclase composition in the Grader intrusion is shown in Fig. 3. The highest An value ($An_{49.2}$) is situated at the top of the pi-C, the An content decreases in the pia-C unit, and is nearly constant at ca. An_{46} in the (gabbro-)noritic unit.

4.2.2. Pyroxenes

Orthopyroxene in hole GRD02-03 (Table 2) displays a restricted range of composition (Fig. 3), with Mg# varying from 66.7 to 63.2. The average Mg# in norite (piahm-C) is 66.1±0.5. The most noticeable variation of orthopyroxene composition occurs in samples at 40 and 37 m deep where Mg# is shifted to more evolved compositions (Mg#=64.3 and 63.2, respectively). Clinopyroxene compositions (Table 3) also show a decrease in Mg# between 37 and 40 m deep.

4.2.3. Fe–Ti oxides

The bulk compositions of ilmenite (ilmenite+exsolved hematite) analysed by XRF on mineral separates from hole GRD02-03 (Table 4) display systematic compositional variation with stratigraphy (Fig. 5). The fraction of

Table 4
XRF analyses of separated ilmenite in hole GRD02-03 in the Grader layered intrusion

Depth (m)		SiO_2	TiO_2	Al_2O_3	Fe_2O_{3tot}	FeO	Fe_2O_3	MnO	MgO	Total	Xgeik	Xpyr	Xhem	Xilm	Ni	V	Cr	Zn	Zr	Nb
10	piahm-C	0.34	41.54	0.19	59.21	21.03	34.36	0.44	1.43	99.33	0.054	0.009	0.201	0.735	31	1164	9	108	47	41
30	piahm-C	0.30	40.39	0.24	59.44	23.38	32.44	0.43	1.93	99.11	0.073	0.009	0.224	0.694	22	1170	7	135	40	44
50	piahm-C	0.38	38.58	0.18	61.81	26.77	31.53	0.34	1.58	99.36	0.060	0.007	0.257	0.676	41	1441	44	88	62	50
80	piahm-C	0.28	35.93	0.12	64.04	31.53	29.26	0.25	1.57	98.94	0.060	0.005	0.305	0.630	36	1620	47	72	20	51
110	piahm-C	0.29	37.28	0.15	63.18	29.68	30.15	0.29	1.73	99.57	0.066	0.006	0.284	0.644	30	1527	33	97	7	47
135	piahm-C	0.28	35.68	0.14	65.41	32.82	29.33	0.26	1.40	99.91	0.053	0.006	0.315	0.627	52	1683	130	81	0	39
140	pia-C	0.25	35.21	0.10	65.37	33.70	28.50	0.15	1.69	99.60	0.064	0.003	0.323	0.609	27	1912	348	8	49	34
160	pia-C	0.35	36.65	0.19	63.85	30.65	29.87	0.14	1.65	99.50	0.063	0.003	0.294	0.640	54	1986	491	0	0	24
175	pi-C	0.04	39.66	0.03	60.50	25.98	31.06	0.13	2.51	99.41	0.094	0.003	0.247	0.656	125	2326	743	0	0	8
182	pi-C	0.00	38.84	0.03	61.76	27.83	30.53	0.12	2.40	99.75	0.090	0.003	0.264	0.644	117	2307	832	0	0	8
190	pi-C	0.53	36.96	0.24	62.78	27.76	31.51	0.14	0.89	98.03	0.035	0.003	0.272	0.690	236	2034	456	22	0	11
193	pi-C	0.00	38.39	0.00	61.91	28.41	30.15	0.13	2.38	99.46	0.090	0.003	0.270	0.637	95	2113	873	0	16	12

Major elements in weight percent, FeO and Fe_2O_3 recalculated from Fe_2O_{3tot} by charge balance; molar fractions of geikielite, pyrophanite, hematite and ilmenite (Xgeik, Xpyr, Xhem, Xilm) calculated following QUILF algorithm (Andersen et al., 1993); trace elements in parts per million (ppm).

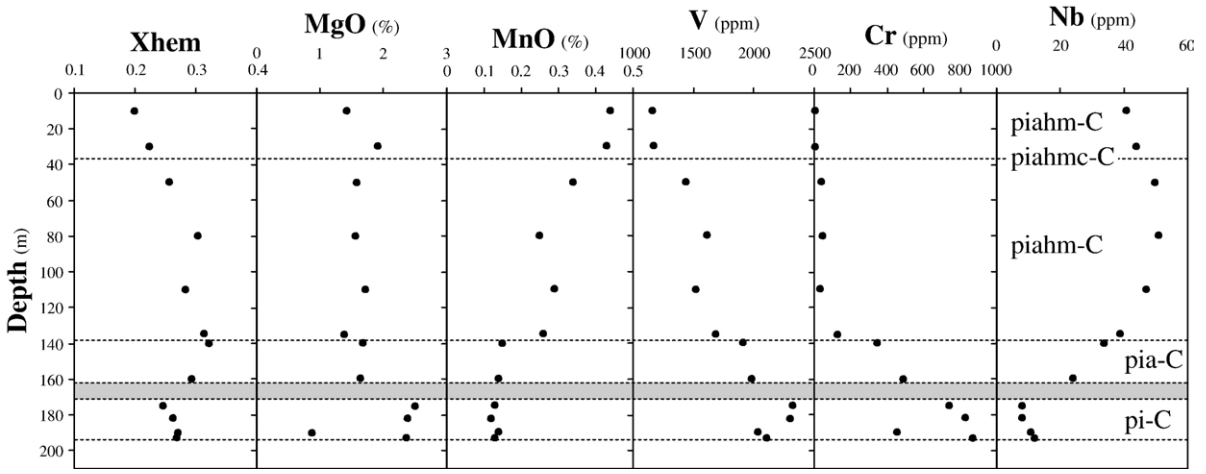

Fig. 5. Stratigraphic variation of ilmenite compositions in hole GRD02-03. The grey line represents the 9 m-thick anorthosite layer.

hematite in ilmenite (X_{hem}) varies from 0.20 to 0.32, with maximum values in samples around 140 m deep. The MgO content in ilmenite is 2.4 wt.% at the base of the intrusion, except in sample at 190 m in which ilmenite is strongly altered (Fig. 4B). From 160 m up to the top of the intrusion, the MgO content of ilmenite is nearly constant between 1.4 and 1.7 wt.%. V and Cr contents of ilmenite decrease up-section while MnO and Nb increase.

The major element composition of magnetite is nearly constant in the studied borehole (Table 5). Magnetite is Ti-poor (ca. 2 wt.% TiO_2) at the base of the noritic unit at 135 m and <0.6 wt.% above. The V content of magnetite ranges from 2500 to 2300 ppm, which is about twice that of ilmenite in the same sample. Ni and Cr contents globally decrease up-section with an irregular pattern (Table 5).

4.2.4. Apatite

The concentrations of Ce (and all other REE), Y, and Sr in liquidus apatite (Table 6) increase continuously up-section and reach maximum values at 30–50 m deep (Fig. 6A). Ce (and the REE) slightly decreases above 50 m and Y and Sr above 30 m. The REE contents in apatite normalized to chondrites (Fig. 6B) are characterized by a LREE-enrichment (La/Yb_N=12.3–14.3) with a small negative Eu anomaly (Eu/Eu*=0.75–0.78).

4.3. Whole rock compositions

Fig. 7 displays the variation of whole rock compositions with stratigraphy in three selected holes: GRD02-03 (Table 7), -05 and -09 are the longest sections through the intrusion. Bulk compositions determined for samples from other holes penetrating shorter sections (and not reported here) have similar patterns that can be easily correlated with the longer cores.

The successive appearance of phases in the Grader intrusion (Fig. 3) is recorded in the whole rock geochemistry (Fig. 7). The most striking characteristics in GRD02-03 are the increase in P_2O_5 due to the appearance of cumulus apatite and the abrupt shift in

Table 5
XRF analyses of separated magnetite in hole GRD02-03 in the Grader layered intrusion

Depth (m)		SiO_2	TiO_2	Al_2O_3	Fe_2O_3	FeO	MnO	MgO	Total	Usp	Ni	V	Cr	Zn	Mn
10	piahm-C	0.24	0.37	0.71	67.64	30.92	0.00	0.38	100.26	0.011	160	2327	65	567	148
30	piahm-C	0.19	0.00	0.81	68.55	30.83	0.00	0.33	100.71	0.000	136	2305	61	528	160
50	piahm-C	0.09	0.62	0.63	66.49	30.95	0.01	0.29	99.08	0.018	205	2498	133	551	169
80	piahm-C	0.12	0.56	0.59	67.08	31.06	0.00	0.30	99.71	0.016	362	2428	227	724	122
110	piahm-C	0.08	0.18	0.64	67.25	30.53	0.00	0.28	98.96	0.005	370	2494	185	613	125
135	piahm-C	0.18	2.02	0.60	63.82	32.17	0.01	0.33	99.13	0.059	551	2409	323	614	171

Major elements in weight percent, FeO and Fe_2O_3 recalculated from Fe_2O_{3tot} by charge balance; molar fractions of ulvöspinel (Usp) calculated following QUILF algorithm (Andersen et al., 1993); trace elements in parts per million (ppm).

Table 6
Trace element compositions (ppm) of separated apatite in hole GRD02-03 in the Grader layered intrusion (ICP-MS analyses) and partition coefficients between apatite and melt

Depth (m)	10	30	50	80	110	135	140	160	D_i*
	piahm-C	piahm-C	piahm-C	piahm-C	piahm-C	piahm-C	pia-C	pia-C	
Mn	241	284	289	275	296	270	335	439	
Sr	505	522	520	495	521	501	481	472	
Y	312	343	342	330	327	300	289	222	
La	241	238	280	262	254	238	237	136	3.9
Ce	688	724	808	750	746	683	690	425	4.7
Pr	114	124	132	124	123	110	112	74.5	5.4
Nd	564	618	637	597	606	541	538	386	6.0
Sm	107	115	118	112	114	101	101	75.9	6.6
Eu	26.5	28.0	28.5	27.0	27.3	25.1	23.5	18.3	3.9
Gd	104	113	113	109	108	98.2	93.3	75.0	6.8
Tb	13.2	14.6	14.8	14.3	13.9	12.8	12.2	9.40	6.1
Dy	63.9	69.7	70.0	67.2	65.9	61.3	58.1	45.0	5.3
Ho	9.68	10.5	10.4	10.1	9.84	9.20	8.72	6.46	4.6
Er	21.8	23.0	23.9	23.2	22.3	20.9	19.7	14.2	4.0
Yb	11.9	12.1	12.7	13.0	12.3	11.8	11.0	7.15	3.4
Eu/Eu*	0.77	0.76	0.76	0.75	0.76	0.78	0.75	0.75	
(La/Yb)N	13.1	12.7	14.3	13.0	13.4	13.0	13.9	12.3	

* Partition coefficients between apatite and melt from Charlier et al. (2005).

MgO due to the appearance of cumulus orthopyroxene. In the other holes, the deepest samples are P_2O_5-rich and thus the plagioclase-ilmenite cumulates (pi-C), which are present in the first 32 m of GRD02-03, are missing. In holes GRD02-05 and -09, the lowermost cumulates contain apatite and can be correlated with pia-C, lying above the anorthosite layer at 162 m in GRD02-03.

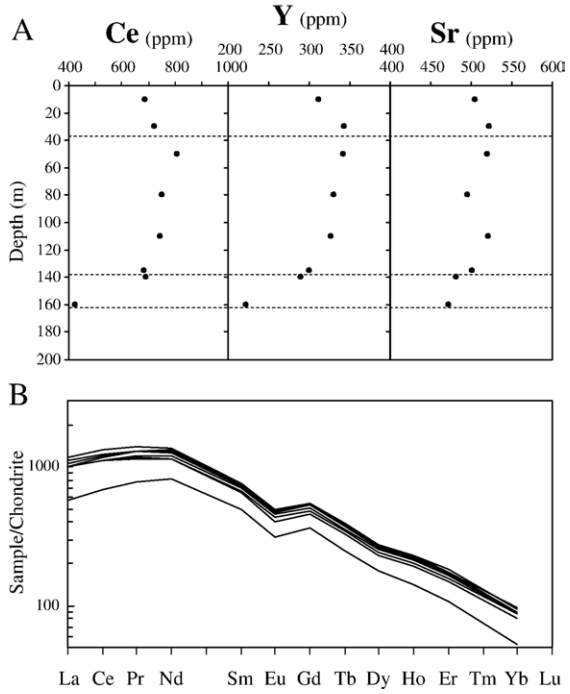

Fig. 6. (A) Stratigraphic variation of apatite composition in hole GRD02-03. (B) Chondrite-normalized REE compositions of separated apatites (after Sun and McDonough, 1989).

In pi-C at the base of hole GRD02-03, the proportion of the two phases is highly variable, resulting in rocks ranging from anorthosite to massive ilmenite. Another noticeable characteristic is the very low P_2O_5 concentration indicating the absence of apatite. Above this level in GRD02-03, the evolution of whole rock compositions is similar to that observed in the other two drill cores. The most significant compositional variations include: (1) a "Z-shaped" variation of P_2O_5 content at the base followed by a relatively constant concentration of ca. 4 wt.% P_2O_5; (2) an abrupt shift from MgO-poor rocks (<2 wt.% MgO) to rocks richer in MgO (6–7 wt.%) and a significant decrease in MgO within zones starting at 38 m, 60 m and 90 m in GRD02-03, -05 and -09 respectively; (3) maximum values of K_2O and Al_2O_3 and low values of Fe_2O_3 and TiO_2 in these thin zones in each drill core; and (4) a gabbronoritic horizon in the upper part of each hole defined by the presence of cumulus clinopyroxene (Fig. 3), followed by a reverse evolution in geochemical trends.

4.4. Fine-grained ferrodiorites in dykes

A 10–15 cm-thick fine-grained dyke that cross-cuts the layered rocks was sampled in outcrops along the

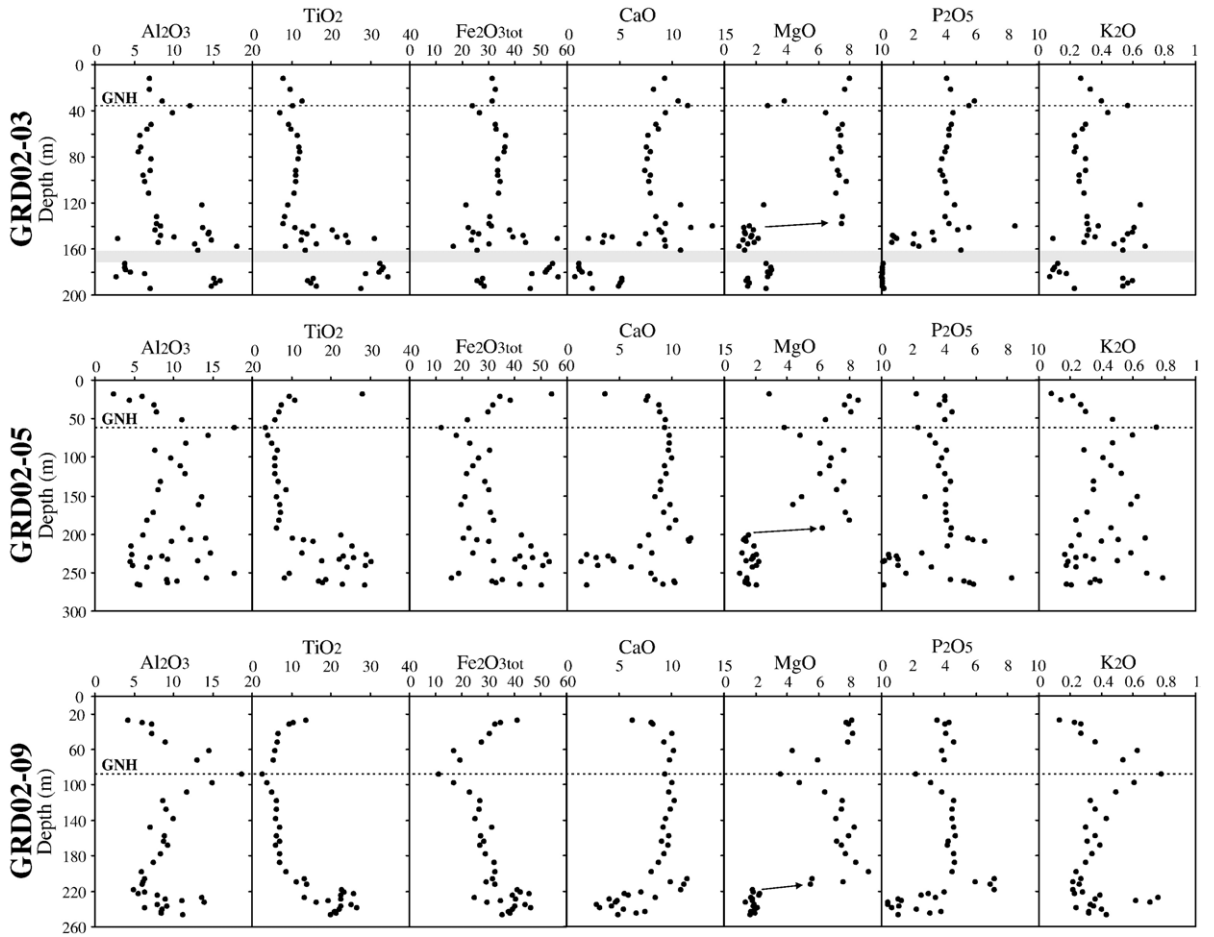

Fig. 7. Stratigraphic variation for whole rock major element compositions in drill holes GRD02-03, -05 and -09. GNH is the Gabbronoritic Horizon and the arrow indicates the abrupt increase in MgO content in the lower part of each hole. The grey line in GRD02-03 represents the 9 m-thick anorthosite layer.

railroad. Several drill cores in the Grader intrusion have cross-cut similar discordant fine-grained rocks. The rock is equigranular and the mineralogy is mainly antiperthitic plagioclase, orthopyroxene, clinopyroxene, ilmenite, magnetite and small elongated apatite. Bulk compositions (Table 8) reveal ferrodioritic

Table 7
Major element compositions of selected whole rock in hole GRD02-03 in the Grader layered intrusion

Depth (m)	SiO_2	TiO_2	Al_2O_3	Fe_2O_3	MnO	MgO	CaO	Na_2O	K_2O	P_2O_5	LOI	Total
WR 10–12	30.50	7.92	7.01	31.45	0.21	8.00	9.33	1.30	0.27	4.12	−0.78	99.33
WR 30–32	24.40	12.80	8.57	31.45	0.18	3.82	10.60	1.72	0.40	5.92	−0.67	99.19
WR 34–36	30.80	10.30	12.10	23.88	0.14	2.79	11.50	2.49	0.57	5.58	−0.43	99.72
WR 50–52	29.20	9.21	7.14	32.74	0.28	7.53	8.52	1.30	0.30	4.44	−0.89	99.77
WR 80–82	27.80	11.70	7.21	33.60	0.23	6.86	7.68	1.40	0.30	3.85	−1.02	99.61
WR 110–112	27.80	10.80	6.84	33.88	0.26	7.13	7.97	1.30	0.29	4.13	−0.94	99.46
WR 136–138.2	31.40	7.82	7.88	30.17	0.27	7.48	9.39	1.56	0.31	4.31	−0.75	99.84
WR 140–142	30.70	11.00	13.70	22.30	0.07	1.27	11.80	2.78	0.61	5.55	−0.26	99.52
WR 158–161.3	27.30	13.50	13.10	25.74	0.08	1.33	10.80	2.64	0.54	5.07	−0.17	99.93
WR 174–176	6.04	33.30	3.85	53.33	0.14	2.99	1.10	0.51	0.10	0.03	−2.00	99.39
WR 182–184.2	3.51	34.50	2.77	56.62	0.14	2.80	0.79	0.34	0.07	0.02	−2.26	99.30
WR 190–192.3	30.10	16.30	14.80	28.45	0.08	1.52	4.93	2.83	0.54	0.06	−0.07	99.54
WR 192.3–194.7	13.30	27.70	7.06	46.04	0.13	2.66	2.42	1.19	0.23	0.13	−1.23	99.63

affinities; they have high FeO_{tot} (16.84–21.77 wt.%) and TiO_2 (3.90–6.20 wt.%) contents and are also P_2O_5-rich (2.69–3.86 wt.%). Similar compositions are commonly interpreted as liquids associated with massif-type anorthosites (e.g. Vander Auwera et al., 1998b).

Table 8
Major and trace element compositions of fine-grained dykes associated with the Grader layered intrusion

	145–937	145–938	223–601	223–604	225–135	145–648	225–302
Major elements (wt.%)							
SiO_2	38.99	38.53	39.71	39.52	37.72	40.13	52.54
TiO_2	4.57	4.40	3.90	6.20	5.15	4.57	4.26
Al_2O_3	13.66	13.12	12.70	14.97	11.92	13.57	13.36
Fe_2O_{3tot}	20.92	21.77	21.89	16.84	20.97	19.94	14.53
MnO	0.20	0.22	0.22	0.07	0.20	0.18	0.15
MgO	4.29	4.47	4.89	5.30	5.20	5.09	2.83
CaO	10.41	10.45	11.23	9.39	11.24	9.48	5.06
Na_2O	2.43	2.48	2.45	2.87	2.18	2.71	3.26
K_2O	0.46	0.47	0.41	0.48	0.34	0.52	2.22
P_2O_5	3.30	3.28	2.69	3.05	3.86	2.88	0.78
Total	99.24	99.18	100.09	98.70	98.78	99.07	98.98
Trace elements (ppm)							
U	0.17	0.17	0.05	0.04	0.10	0.12	0.32
Th	1.13	1.45	0.60	1.15	0.79	1.25	1.30
Pb	6.5	13.4	2.3	6.7	2.2	3.0	11.2
Zr	190	197	147	163	147	151	376
Hf	4.55	4.31	4.33	5.31	4.32	4.41	9.47
Nb	17.3	20.4	17.2	19.2	17.6	21.6	19.2
Ta	1.17	1.07	0.91	1.49	1.06	1.23	1.37
Rb	3.23	3.07	1.23	2.98	0.32	3.00	30.0
Sr	688	718	637	669	698	592	642
Ba	305	394	309	301	235	325	945
Ni	27	30	50	93	28	56	27
V	250	287	251	337	233	283	150
Cr	15.6	28.5	5.9	42.4	6.3	24.0	7.6
Zn	222	261	263	85	213	200	207
Co	58	54	57	51	54	54	34
Cu	56	55	84	31	66	77	33
Ga	31	35	36	38	30	25	27
Y	50.6	66.6	59.8	66.4	47.1	54.0	25.0
La	51.1	56.6	40.6	54.3	49.9	58.0	34.2
Ce	134	145	108	141	122	144	81
Pr	20.9	22.8	16.0	22.4	19.0	20.7	11.8
Nd	82.5	96.2	74.1	91.2	90.8	91.2	50.8
Sm	18.4	21.9	16.1	18.3	18.7	18.6	13.2
Eu	4.19	5.43	4.25	4.15	5.18	4.45	4.06
Gd	14.9	17.2	15.4	17.0	15.1	16.4	9.46
Tb	2.22	2.26	2.17	2.55	1.98	2.13	1.33
Dy	11.6	13.0	11.7	12.7	10.0	10.7	6.5
Ho	2.06	2.23	2.09	2.40	1.91	2.03	1.10
Er	4.43	4.85	4.65	5.08	3.97	4.54	2.28
Tm	0.50	0.53	0.49	0.59	0.45	0.54	0.27
Yb	2.90	3.31	3.10	3.16	2.59	3.01	1.39
Lu	0.39	0.43	0.41	0.41	0.36	0.39	0.16
Eu/Eu*	0.78	0.86	0.83	0.73	0.95	0.79	1.12
$(La/Yb)_N$	11.4	11.1	8.5	11.1	12.5	12.5	15.9

Table 8 (*continued*)

	145–937	145–938	223–601	223–604	225–135	145–648	225–302
NNO, 1150 °C, 4 kb							
FeO	15.95	16.60	16.56	12.76	15.94	15.17	
Fe_2O_3	3.21	3.34	3.49	2.67	3.27	3.09	
Density	2.92	2.93	2.93	2.87	2.94	3.00	
NNO + 1, 1150 °C, 4 kb							
FeO	14.66	15.26	15.18	11.70	14.64	13.94	
Fe_2O_3	4.63	4.82	5.03	3.85	4.72	4.46	
Density	2.99	3.01	3.01	2.87	2.93	2.97	

FeO and Fe_2O_3 recalculated from Kress and Carmichael (1991).

4.5. Sr isotopic compositions

Ratios of $^{87}Sr/^{86}Sr$ of the plagioclase (recalculated at 1060 Ma) (Table 9) show a slight difference between the host anorthosite and the Grader deposit with average values of 0.703995 and 0.704319, respectively. Plagioclase in the host anorthosite and the deposit was thus formed from magmas of slightly different isotopic composition. Plagioclase from the anorthosite layer located in GRD02-03 between 171 and 162 m deep has an initial Sr isotope ratio (0.703821) close to that of the host anorthosite, which suggests that the layer of anorthosite is an inclusion of the host anorthosite in the Grader intrusion.

Table 9 also shows the initial Sr isotope ratios of ferrodioritic dykes that cross-cut the intrusion. Samples 145–648 (a typical fine-grained ferrodiorite) and 225–302 (a more evolved ferrodiorite) have initial Sr isotope ratios of 0.705408 and 0.703925, respectively. The first sample, as shown below, has a chemical composition which is in equilibrium with the Grader norite, but is isotopically different, probably slightly contaminated by crustal material. The second sample of ferrodiorites is isotopically similar to plagioclase of the Grader deposit and could thus represent an evolved residual liquid related to the intrusion.

5. Discussion

5.1. The sequence of crystallization and the origin of nelsonite

Several studies have demonstrated that ilmenite is an early liquidus phase in liquids associated with andesine anorthosites. In the Bjerkreim–Sokndal layered intrusion,

ilmenite appears as the second liquidus phase after plagioclase (Wilson et al., 1996). In the Tellnes ilmenite deposit (Charlier et al., 2006) and other ore bodies in the Rogaland Anorthosite Province (Duchesne, 1999), ilmenite also appears after plagioclase and before Fe–Mg silicates. The stratigraphic evolution in the Grader intrusion is another example of early saturation of ilmenite. The occurrence of monomineralic layers of ilmenite alternating with plagioclase-rich layers at the base of the intrusion indicates that these two minerals were the first liquidus phases to crystallize.

Another particular feature of the Grader intrusion is the presence of plagioclase–ilmenite–apatite cumulates (pia-C). In some layers where plagioclase is absent or present only in trace amounts, these ilmenite–apatite rocks may be referred to as nelsonites. Nelsonites have typically been interpreted as a product of liquid immiscibility (Philpotts, 1967; Kolker, 1982). However, experiments by Lindsley (2003) have failed to produce immiscible Fe–Ti–P-rich liquids. The interpretation of Dymek and Owens (2001) that nelsonites represent cumulates is supported in this study by the well-defined stratigraphic evolution in the Grader intrusion. The appearance of cumulus apatite after plagioclase and ilmenite and before Fe–Mg silicates (Fig. 3), responsible for the abrupt shift of the P_2O_5 content in the whole rocks (Fig. 7), is a clear evidence that fractional crystallization can produce nelsonites. The shift to P_2O_5-rich cumulates appears earlier in the succession than the shift to MgO-rich cumulates, which marks the appearance of cumulus orthopyroxene.

It is possible that saturation of apatite may even occur with plagioclase and before ilmenite in liquids with a similar and higher P_2O_5 concentration but with a lower TiO_2 content. This sequence of crystallization would explain the occurrence of a massive, hundred meters-thick unit of apatite-bearing anorthosite, averaging 7 wt.% P_2O_5, in the northern part of the Lac-Saint-Jean anorthositic suite (Hébert et al., 2003).

5.2. Rayleigh fractionation and cotectic proportion of ilmenite

Ilmenite compositions in hole GRD02-03 (Fig. 5) displays systematic stratigraphic variations. The continuous decrease in compatible element concentrations (e.g. V and Cr) and the increase in incompatible element concentrations (e.g. MnO and Nb) suggest that fractional crystallization was the main mechanism of differentiation. The trend of ilmenite compositions in a log Cr vs. log V diagram (Fig. 8A) is consistent with fractional crystallization following the equation of Rayleigh (1896): $C_i^{\mathrm{Liq}} = C_i^0 F^{(D-1)}$ where C_i^{Liq} is the instantaneous concentration of element i in the melt, C_i^0 is the initial concentration of element i in the parental magma, F is the fraction of residual liquid, and D is the bulk partition coefficient between the cotectic cumulate minerals and the liquid (i.e. $D = \sum X^j D_i^j$ where X^j is the cotectic mass fraction of mineral j in the cumulate, and D_i^j is the partition coefficient of element i between mineral j and melt). Due to the exponential nature of the Rayleigh equation, samples related to each other by fractional crystallization will plot on linear trends in log–log diagrams when the bulk partition coefficient is constant. In Fig. 8A, ilmenite from all cumulus assemblages in the Grader intrusion can statistically be considered to plot on a single linear trend ($r^2 = 0.96$). This implies that the bulk partition coefficients for Cr and V for the different fractionating cumulus assemblages did not significantly differ. This results from both high values of the ilmenite partition coefficients for V and Cr and from the high modal proportions of ilmenite compared to other liquidus phases. This in turn means that the cotectic proportion of ilmenite must remain

Table 9
Sr isotopic composition of ferrodiorites and plagioclases from the Grader layered intrusion and the host anorthosite

		Rb (ppm)	Sr (ppm)	$^{87}Sr/^{86}Sr$	Error (+/−2s)	$^{87}Rb/^{86}Sr$	$(^{87}Sr/^{86}Sr)$ at 1060 Ma
145–648	Ferrodiorite	3.0	618	0.705622	0.000009	0.0140	0.70541
225–302	Ferrodiorite	30	642	0.705977	0.000008	0.1352	0.70393
HSP-AN 01	HSP anorthosite	1.92	1223	0.704011	0.000007	0.0045	0.70394
GRD02-10 at 4 m	Roof anorthosite	4.93	1139	0.704335	0.000007	0.0125	0.70415
GRD02-03 at 203 m	Floor anorthosite	1.42	1231	0.703948	0.000007	0.0033	0.70390
GRD02-03 at 170 m	Anorthosite septum	1.79	1156	0.703889	0.000007	0.0045	0.70382
GRD02-03 at 50 m	Norite (piahm-C)	3.26	1297	0.704448	0.000008	0.0073	0.70434
GRD02-03 at 50 m *	Norite (piahm-C)	–	–	0.704453	0.000006	0.0073	0.70434
GRD02-03 at 160 m	Nelsonite (pia-C)	0.88	1335	0.704519	0.000006	0.0019	0.70449
GRD02-03 at 193 m	Massive oxide (pi-C)	1.77	1153	0.704175	0.000008	0.0044	0.70411

* Duplicate.

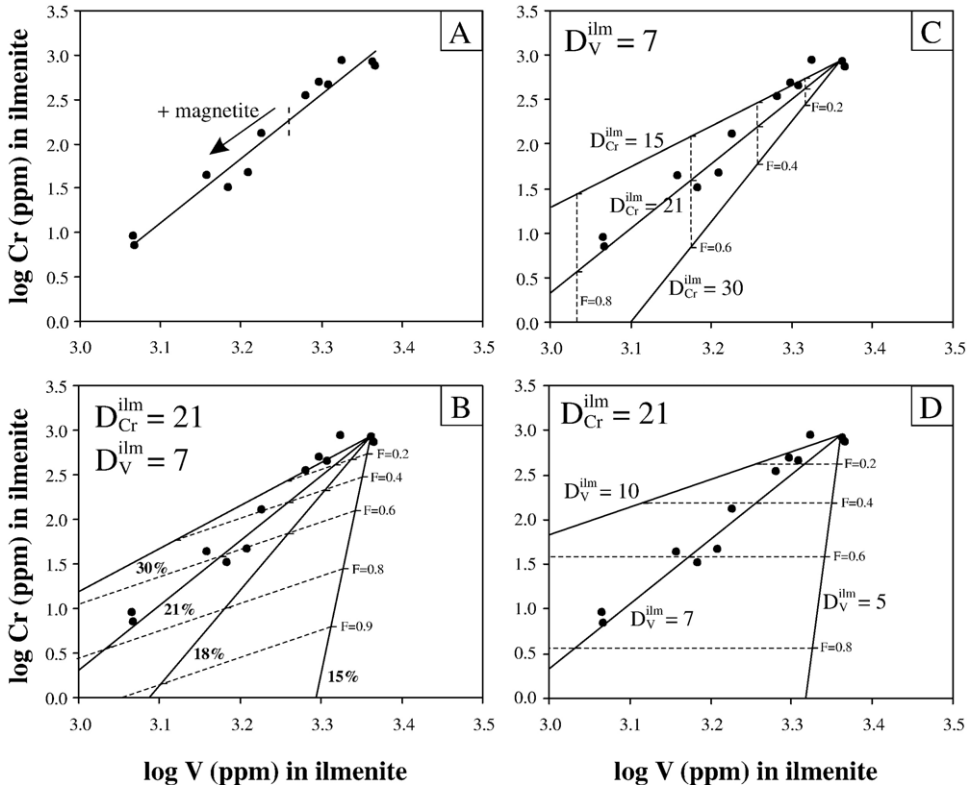

Fig. 8. (A) log V vs. log Cr in ilmenite in hole GRD02-03 of the Grader layered intrusion with the linear regression ($r^2 = 0.96$). The dashed line marks the appearance of cumulus magnetite; (B) Results of calculations for Cr and V concentrations in ilmenite using a cotectic proportion of ilmenite of 21 wt.% and various cotectic proportions of ilmenite (15, 18, 21 and 30 wt.%); (C–D) Results of calculation for Cr and V concentrations in ilmenite using various D_V^{Ilm} and D_{Cr}^{Ilm}. F is the fraction of residual liquid.

roughly constant with differentiation. Even in piahm-C, the appearance of magnetite, in which V and Cr are commonly highly enriched, does not induce significant variations of D_V^{Bulk} and D_{Cr}^{Bulk} because of the low abundance of cumulus magnetite (<5 vol.%).

Application of the Rayleigh equation permits a quantitative assessment of the cotectic proportion of ilmenite that crystallized, which controls D_V^{Bulk} and D_{Cr}^{Bulk}. By using $D_V^{Bulk} = 7$, consistent with the results of Jang and Naslund (2003) and Duchesne et al. (2006) for similar melt compositions, the slope of the linear regression in Fig. 8A, which corresponds to $(D_{Cr}^{Bulk} - 1)/(D_V^{Bulk} - 1)$, is reproduced using $D_{Cr}^{Ilm} = 21$ and a cotectic proportion of ilmenite of 21 wt.% (Fig. 8B). This calculation is very sensitive to even small variations of the ilmenite cotectic proportion. The influence of variable D_V^{Ilm} and D_{Cr}^{Ilm} (Fig. 8C–D) shows that the trend displayed by ilmenite composition cannot be reproduced with different partition coefficients. Because ilmenite contains 37.9 wt.% TiO_2 on average (Table 4), this cotectic proportion of ilmenite of 21 wt.% corresponds to 8 wt.% TiO_2 in the bulk cotectic cumulate.

5.3. Oxygen fugacity and early saturation of ilmenite

The high hematite content in ilmenite in the Grader intrusion (Fig. 5) is an indicator of a high oxygen fugacity (fO_2) in the magmas from which the ilmenite crystallized. Experimental studies on the stability fields of Fe–Ti oxides (Snyder et al., 1993; Toplis and Carroll, 1995) have shown that at high fO_2, the magnetite–ulvöspinel solid solution precedes the appearance of the ilmenite–hematite solid solution, whereas this order is reversed at low fO_2 in typical basaltic systems. However, ilmenite is the first liquidus Fe–Ti oxide in the Grader intrusion and remains modally more abundant compared to magnetite when it is present. This is explained by another conclusion of Toplis and Carroll (1995) that fO_2 only affects the stability field of magnetite, whereas the crystallization of ilmenite as the first oxide is controlled primarily by the TiO_2 content of the melt. The early saturation of hematite-rich ilmenite in the Grader intrusion instead of Ti-magnetite is thus a reflection of the TiO_2 content of the Grader parental magma being higher than those

studied by Snyder et al. (1993) and Toplis and Carroll (1995).

The general range of oxygen fugacity during crystallization of the Grader intrusion may be estimated from the experimental calibration of the Fe–Ti oxide thermo-oxybarometer of Lattard et al. (2005). Liquidus temperatures during crystallization of the Grader cumulates are estimated to be between 1100 and 1200 °C by analogy with experimental studies on similar compositions (Vander Auwera and Longhi, 1994; Vander Auwera et al., 1998b). In this range of temperature, the fO_2 obtained for ilmenite composition in Grader ($Hem_{20–32}$) (in equilibrium with magnetite or as a single phase) varies between NNO+0.5 and NNO+1.

The negligible effect of the appearance of magnetite on D_V^{Bulk} and D_{Cr}^{Bulk} in the Grader intrusion is consistent with the high fO_2 of the melt. Indeed, Toplis and Corgne (2002) have shown that V and Cr partitioning is strongly dependent on fO_2, which determines the relative proportion of the different 3+, 4+ and 5+ ions; the result is decreasing partition coefficients with oxidizing conditions. At NNO+1 in a P-bearing system, $D_V^{Mt}=11$ (Toplis and Corgne, 2002), which is not significantly different than the $D_V^{Ilm}=7$ in our calculations. The high fO_2 probably had a minor effect on D_V^{Ilm} and D_{Cr}^{Ilm} because ilmenite is known to include highly charged cations such as Nb and Ta (Green and Pearson, 1987) more easily than does magnetite.

5.4. Evidence for the occurrence of a sandwich horizon

A sandwich horizon is the level where cumulates crystallized from the bottom of the intrusion meet those crystallized from the roof (Wager and Brown, 1968). Rocks from a sandwich horizon should thus contain the most evolved minerals of the sequence. The presence of a sandwich horizon has been most effectively documented in the Skaergaard layered intrusion at the level where the Upper Border Series and Layered Series converge (e.g. McBirney, 1995).

In the Grader layered intrusion, a number of observations suggest the existence of such a sandwich horizon. The most evolved mineral compositions are not observed at the top of hole GRD02-03, but around 40–35 m below where orthopyroxene with the lowest Mg# occurs (Fig. 3). This is further supported by the trend to relatively high Ce content of apatite at this depth (Fig. 6) and by several characteristics of the whole rock compositions (Fig. 7). As previously mentioned, this level between 35 and 40 m in GRD02-03 is marked by a more leucocratic character with higher Al_2O_3 and K_2O contents and lower Fe_2O_3, MgO and TiO_2 contents. Similar trends are also observed in GRD02-05 at ca. 60 m deep and in GRD02-09 at ca. 90 m deep. All of these observations indicate that this particular level has the most evolved compositions of the entire Grader intrusion.

5.5. Ferrodiorite dykes: melts in equilibrium with noritic cumulates

The relationship between the fine-grained dykes cross-cutting the Grader intrusion and melt compositions in equilibrium with the cumulates can be evaluated from the composition of cumulus apatite in the intrusion. The REE content of melts in equilibrium with apatite-bearing noritic cumulates can be determined by inverting the composition of cumulus apatite using the equation $C_{REE}^{Liq}=C_{REE}^{Ap}/D_{REE}^{Ap}$. Empirically determined partition coefficients for REE between apatite and melt (D_{REE}^{Ap}) from Charlier et al. (2005; Table 8) are used. They were calculated from gabbro-noritic cumulates from the Bjerkreim–Sokndal layered intrusion, which have a very similar mineralogy to the Grader cumulates. REE of ferrodioritic dykes are plotted in Fig. 9 along with patterns calculated for liquids in equilibrium with apatite. Strong similarities between their absolute REE contents as well as their REE patterns suggest that the ferrodioritic dykes were in equilibrium with oxide apatite norites. The inversion calculation does not reproduce the small negative Eu anomaly of ferrodioritic dykes, but gives a positive Eu anomaly for liquids in equilibrium with apatite. The D_{Eu}^{Ap} of Charlier et al. (2005) is thus different from the value characteristic of the Grader intrusion. D_{Eu}^{Ap} is sensitive to the relative proportion of Eu^{3+} and Eu^{2+} of the melt, and thus to fO_2, because $D_{Eu3+}^{Ap}>D_{Eu2+}^{Ap}$ (Roelandts

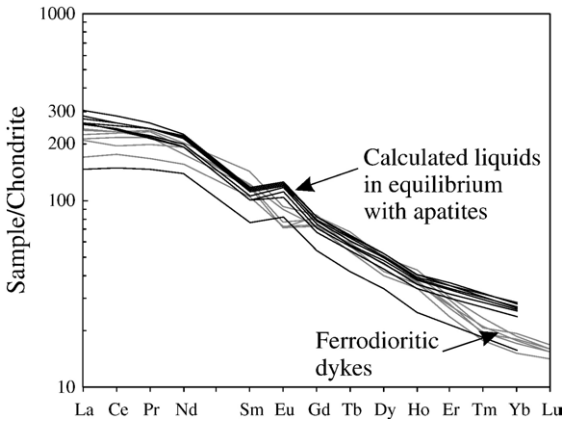

Fig. 9. REE patterns normalized to chondrites (Sun and McDonough, 1989) for ferrodiorite dykes compared to calculated liquids from the inversion of apatite compositions.

and Duchesne, 1979), contrarily to what is observed for plagioclase (Drake and Weill, 1975; Aigner-Torres et al., 2007). In accordance with the higher hematite content of ilmenite in the Grader intrusion (X_{Hem}=0.20–0.32) compared to ilmenite in the Bjerkreim–Sokndal layered intrusion where X_{Hem} varies between 0.03 and 0.19 (Duchesne, 1972), we conclude that D_{Eu}^{Ap} is also higher in the Grader intrusion, because the higher fO_2 of the melt resulted in a higher ratio of Eu^{3+}/Eu^{2+}.

The temperature of apatite saturation in these ferrodioritic melts, calculated from the formulation of Tollari et al. (2006), ranges from 980 to 1080 °C (Table 8). These temperatures compare closely with the liquidus temperature of similar melts (≤1080 °C, Vander Auwera et al., 1998b) and further support the early crystallization of apatite in the stratigraphic sequence.

5.6. Mechanism for ilmenite enrichment: segregation of plagioclase by flotation

The average composition of noritic cumulates may be compared to the composition of the ferrodioritic dykes to evaluate the extent to which the intrusion remained closed during crystallization of the parental magma, i.e. whether the composition of the cumulate pile matches that of ferrodiorites. Average bulk rock compositions for the noritic unit (piahm(±c)-C) and for pi-C+pia-C in holes GRD02-03, -05 and -09 are reported in Fig. 10. It is clear that there is no match between the compositions of the average noritic cumulates and the ferrodiorite compositions. However, there are colinear relations between the compositions of oxide–apatite (gabbro-)norite, ferrodiorites, and plagioclase. This means that some plagioclase may be added to the (gabbro-)norites to obtain the average composition of the ferrodiorites. The high proportion of ilmenite in cumulate rocks of the Grader intrusion thus appears to be the result of the removal of plagioclase from the parental liquid. The mechanism responsible for ilmenite enrichment/plagioclase removal is probably segregation by flotation. The density of plagioclase, which ranges between 2.61 and 2.65 g cm^{-3} for An_{60-40} (Campbell et al., 1978), is commonly less dense than the liquid from which it crystallizes in Proterozoic

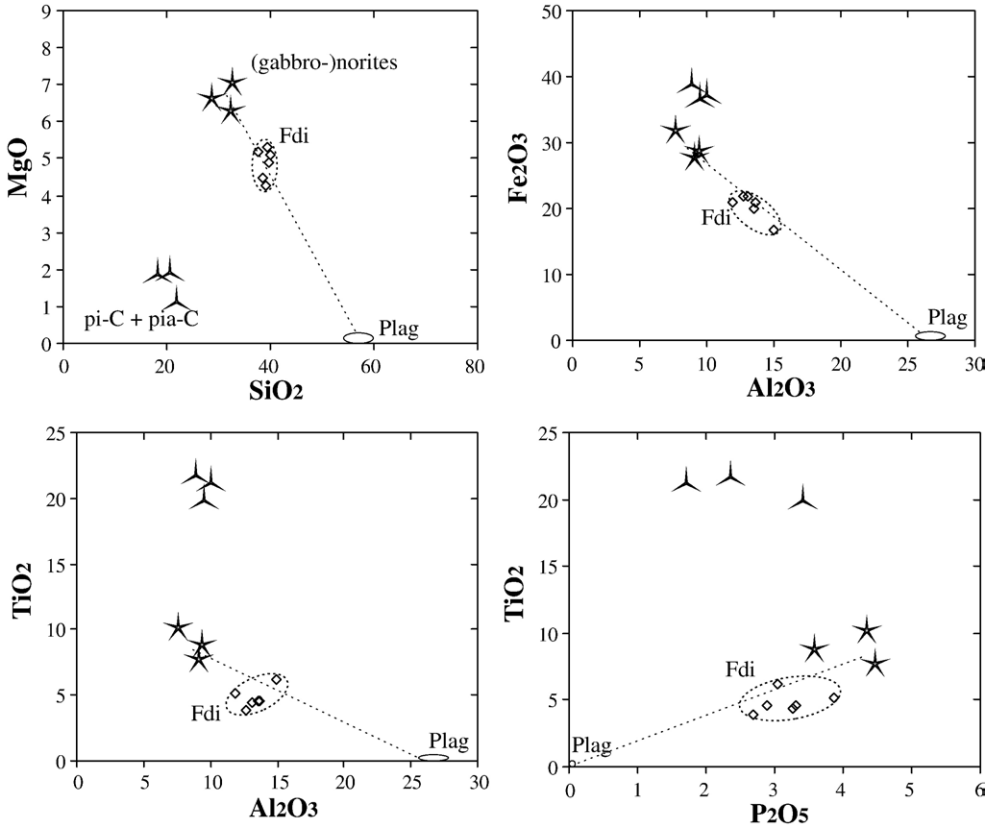

Fig. 10. Binary major element variation diagrams of whole rocks in holes GRD02-03, -05 and -09 in the Grader layered intrusion. The compositional range of plagioclase (plag) is represented by an elliptic area. Open diamonds are ferrodiorite compositions (Fdi).

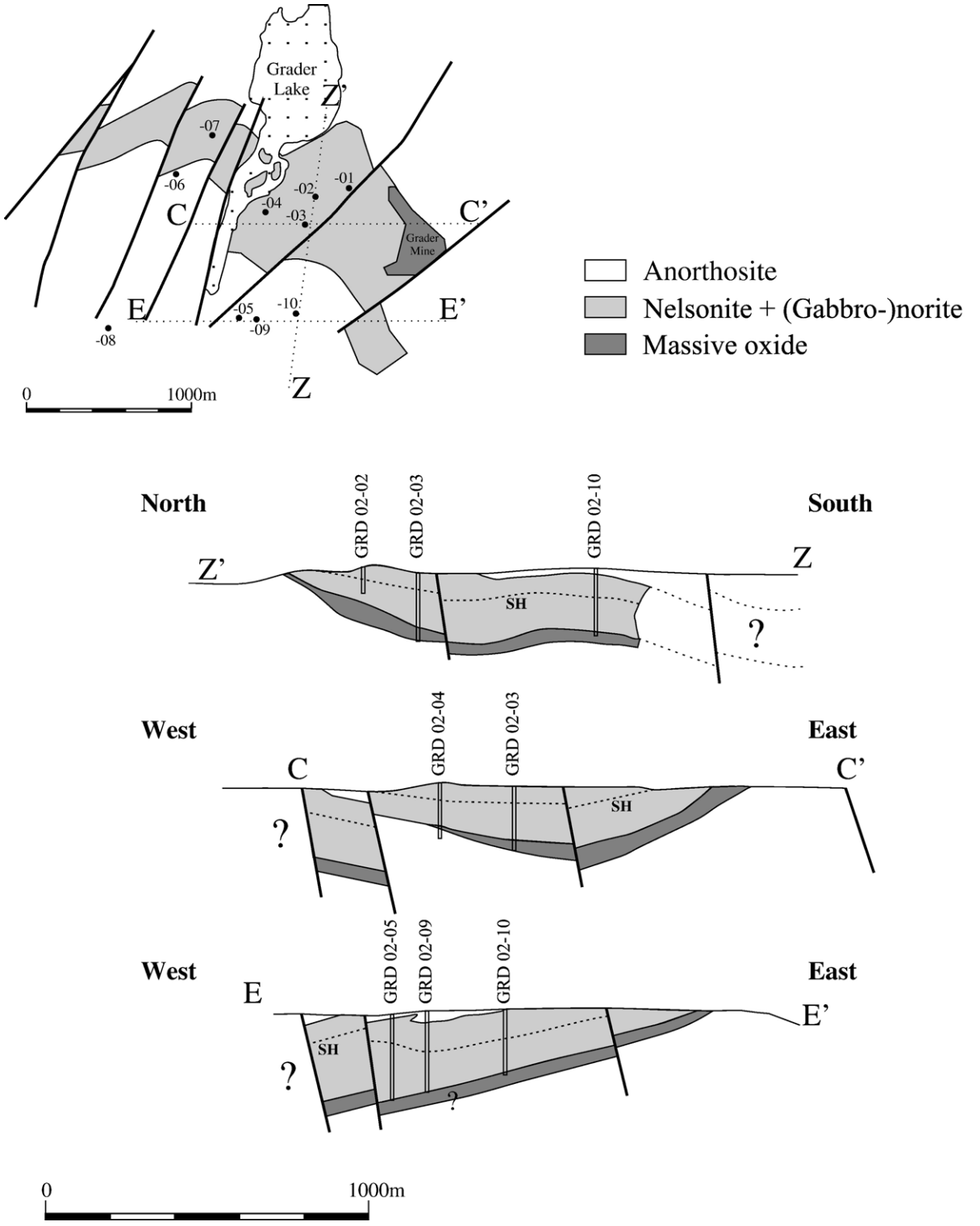

Fig. 11. Cross sections through the Grader layered intrusion with the interpretation of lateral extensions of different ore types. SH is the Sandwich Horizon.

anorthosites (Vander Auwera and Longhi, 1994; Scoates, 2000). We have calculated the densities of the ferrodioritc liquids with the model equation of Lange and Carmichael (1990), which expresses molar volumes of silicate melts as linear functions of composition, temperature and pressure. The densities of these ferrodioritic liquids strongly depend on their Fe^{3+}/Fe^{2+} ratio and P_2O_5 content (Toplis et al., 1994). We have used the model of Kress and Carmichael (1991) to calculate the Fe^{3+}/Fe^{2+} ratio. A conservative value of 4 kbar has been estimated for the pressure of emplacement of the Grader intrusion and calculations have been performed for oxygen fugacities at NNO and NNO+1 as inferred from the ilmenite compositions. Under these conditions, the average Fe_2O_3/FeO of the ferrodiorites is 0.20 at NNO and 0.32 at NNO+1. H_2O, CO_2 and *F* contents are very low in magmas associated with massif-type anorthosites (e.g. Morse, 1982) and consequently, these volatile components have thus been ignored in calculating the densities of the Grader ferrodiorites. The calculated densities range from 2.87 to 3.01 g cm^{-3} (Table 8) and are significantly higher than plagioclase density. Settling of individual grains of plagioclase in these ferrodioritic liquids is thus highly unlikely.

This missing plagioclase may have been transported laterally by magmatic flow to other portions of the intrusion, leading to sections with lower TiO_2 concentrations in the bulk cumulates. Indeed, the TiO_2 concentrations do vary systematically from one section to another, as shown by higher TiO_2 in noritic cumulates in GRD02-03 (ca. 10 wt.% TiO_2) versus GRD02-05 and GRD02-09 (6–8 wt% TiO_2). Interesting in this regard is the low-grade hole GRD02-08 in the far southwest (Fig. 2) where several anorthosite layers are present and oxide apatite (gabbro-)norite is entirely absent for about 150 m above 17 m of banded nelsonite. Oxide apatite (gabbro-)norites are substituted by leuconorite with 10 vol.% or less ilmenite. Finally, massive ilmenite is uncommon being supplanted by plagioclase-ilmenite layers with only 40 vol.% ilmenite. Consequently the southern part of the intrusion which has not been drilled may be less economically interesting.

Alternatively, the floating plagioclase could have accumulated at the top of the Grader intrusion where it cannot be distinguished from the host anorthosite. However, the hypothesis that the noritic unit has also crystallized from the roof down, resulting in the formation of a sandwich horizon, precludes plagioclase floating to the top of the intrusion, suggesting instead lateral plagioclase migration.

5.7. Lateral extension of ore types

Outcrop mapping and stratigraphic correlations between the drill holes allow for an interpretation of the 3D-morphology of the Grader layered intrusion. As previously mentioned, the intrusion has a basin-shape. Massive oxide layers present at the base of hole GRD02-03 (ca. 25 m-thick pi-C) outcrop over a wide 100 m surface within and immediately west of the Grader mine, where they show intensive slump-style folding. The 9 m-thick anorthosite layer above massive ilmenite in hole GRD02-03 (Fig. 3) may be correlated with a similar thickness of anorthosite in GRD02-01 (Fig. 2). In GRD02-03, the Sr isotope composition of plagioclase from the anorthosite layer suggests that it is a xenolith of the enclosing anorthosite. Lateral extension of the anorthosite to GRD02-01 suggests that the xenolith has the shape of a septum lying parallel to the lower contact. The first layered nelsonites appear above this anorthosite in holes GRD02-01 and -03, and ca. 650 m to the south, in holes GRD02-05 and -09 (Fig. 7) and in GRD02-10. In the latter holes, massive ilmenite (pi-C) is absent, thus the pi-C probably thins out to the south and to the west. An alternative possibility is that the septum actually extends to the south and west and that drilling was stopped when reaching what was considered to be the floor of the intrusion. This anorthosite layer may thus have been mistaken as the basal host anorthosite unit in holes GRD02-05, -09 and -10. This hypothesis is indicated by question marks in the interpreted cross-sections of the Grader intrusion proposed in Fig. 11. Additional deeper holes would resolve this issue. Above the anorthosite layer, nelsonites (pia-C) are relatively thin and vary from 20 m in thickness in GRD02-03 to ca. 50 m in GRD02-05. The (gabbro-)noritic unit (piahm(±c)-C) has a variable thickness ranging from 150 to 200 m.

6. Conclusion

The diversity of ore types observed in the Grader layered intrusion resulted from the successive appearance of liquidus phases due to a continuous fractional crystallization process. The parental magma of the intrusion was initially saturated in plagioclase+ilmenite due to its high TiO_2 content. This feature is not peculiar to the Grader intrusion but is observed in some cumulate series associated with Proterozoic massif-type anorthosites (e.g. the Bjerkreim–Sokndal layered intrusion; Wilson et al., 1996). The segregation of plagioclase and ilmenite via density differences resulted in the formation of thick massive ilmenite layers at the base of the intrusion. Subsequently, the magma became saturated in

apatite due to the high P_2O_5 content of the parental magmas, and was followed by orthopyroxene, magnetite and clinopyroxene. This atypical early saturation of apatite, associated with the crystallization of ilmenite and the gravitational segregation of ilmenite + apatite relative to plagioclase, was responsible for the formation of nelsonite. There is no petrographic or field evidence to support an origin of the nelsonite by liquid immiscibility. The sequence of cumulus phases and whole rock compositions observed at the base of the intrusion is repeated from the top downward at the top of the intrusion, thus leading to the recognition of a sandwich horizon. The proportion of ilmenite in the studied portion of the Grader layered intrusion is higher than the cotectic proportion of 21 wt.%. Segregation of plagioclase by flotation in a dense ferrodioritic melt, with which noritic cumulates were in equilibrium, was responsible for the relative ilmenite enrichment. This plagioclase was probably transported laterally by magmatic flow to other portions of the intrusion.

Acknowledgements

This work was funded by the Belgian Fund for Joint Research and the Fund for Research in Industry and Agriculture (FRIA). Rio Tinto is gratefully acknowledged for the financial support and permission to publish the data. Guy Bologne is thanked for the assistance with XRF analyses. Comments by Eric Force have been highly appreciated. This paper has benefited from the constructive reviews by John Longhi and James Scoates.

References

Aigner-Torres, M., Blundy, J., Ulmer, P., Pettke, T., 2007. Laser Ablation ICPMS study of trace element partitioning between plagioclase and basaltic melts: an experimental approach. Contributions to Mineralogy and Petrology 153, 647–667.

Andersen, D.J., Lindsley, D.H., Davidson, P.M., 1993. QUILF: a PASCAL program to assess equilibria among Fe–Mg–Ti oxides, pyroxenes, olivine, and quartz. Computers & Geosciences 19, 1333–1350.

Bergeron, M.B., 1986. Minéralogie et géochimie de la suite anorthositique de la région du Lac Allard, Québec: Evolution des membres mafiques et origine des gites massifs d'ilménite. Ph.D. dissertation, Université de Montréal, 480 pp.

Campbell, I.H., Roeder, P.L., Dixon, J.M., 1978. Plagioclase buoyancy in basaltic liquids as determined with a centrifuge furnace. Contributions to Mineralogy and Petrology 67, 369–377.

Charlier, B., Vander Auwera, J., Duchesne, J.-C., 2005. Geochemistry of cumulates from the Bjerkreim–Sokndal layered intrusion (S. Norway): Part II. REE and the trapped liquid fraction. Lithos 83 (3–4), 255–276.

Charlier, B., Duchesne, J.-C., Vander Auwera, J., 2006. Magma chamber processes in the Tellnes ilmenite deposit (Rogaland Anorthosite Province, SW Norway) and the formation of Fe–Ti ores in massif-type anorthosites. Chemical Geology 234 (3–4), 264–290.

Charlier, B., Skår, Ø., Korneliussen, A., Duchesne, J.-C., Vander Auwera, J., 2007. Ilmenite composition in the Tellnes Fe–Ti deposit, SW Norway: fractional crystallization, postcumulus evolution and ilmenite-zircon relation. Contributions to Mineralogy and Petrology 154, 119–134.

Drake, M.J., Weill, D.F., 1975. Partition of Sr, Ba, Eu^{2+}, $Eu^{2+}$and other REE between plagioclase feldspar and magmatic liquid: an experimental study. Geochimica et Cosmochimica Acta 39, 689–712.

Duchesne, J.C., 1972. Iron-titanium oxide minerals in the Bjerkrem–Sogndal Massif, South-western Norway. Journal of Petrology 13 (1), 57–81.

Duchesne, J.C., 1999. Fe–Ti deposits in Rogaland anorthosites (South Norway): geochemical characteristics and problems of interpretation. Mineralium Deposita 34, 182–198.

Duchesne, J.C., Shumlyanskyy, L., Charlier, B., 2006. The Fedorivka layered intrusion (Korosten Pluton, Ukraine): an example of highly differentiated ferrobasaltic evolution. Lithos 89 (3–4), 353–376.

Dymek, R.F., Owens, B.E., 2001. Petrogenesis of apatite-rich rocks (nelsonites and oxide-apatite gabbronorites) associated with massif anorthosites. Economic Geology 96, 797–815.

Emslie, R.F., Hunt, P.A., 1990. Ages and petrogenetic significance of igneous mangerite charnockite suites associated with massif anorthosites, Grenville Province. Journal of Geology 98, 213–231.

Force, E.R., 1991. Geology of Titanium-mineral Deposits, US Geological Survey Special Paper, p. 112.

Green, T.H., Pearson, N.J., 1987. An experimental study of Nb and Ta partitioning between Ti-rich minerals and silicate liquids at high pressure and temperature. Geochimica et Cosmochimica Acta 51, 55–62.

Hargraves, R.B., 1962. Petrology of the Allard Lake anorthosite suite, Quebec, Petrologic studies: a volume to honor A.F. Buddington. Geol. Soc. Am., Denver, pp. 163–189.

Hébert, C., Cadieux, A.-M., van Breemen, O., 2003. Temporal evolution and nature of Ti–Fe–P mineralization in the anorthosite–mangerite–charnockite–granite (AMCG) suites of the south-central Grenville Province, Saguenay – Lac St. Jean area, Quebec, Canada. Canadian Journal of Earth Science 42, 1865–1880.

Irvine, T.N., 1982. Terminology for layered intrusions. Journal of Petrology 23 (2), 127–162.

Jang, Y.D., Naslund, H.R., 2003. Major and trace element variation in ilmenite in the Skaergaard intrusion: petrologic implications. Chemical Geology 193, 109–125.

Kerr, A., Ryan, B., 2000. Threading the eye of the needle: lessons from the search for another Voisey's Bay in Labrador, Canada. Economic Geology 95 (4), 725–748.

Kolker, A., 1982. Mineralogy and geochemistry of Fe–Ti oxide and apatite (nelsonite) deposits and evaluation of the liquid immiscibility hypothesis. Economic Geology 77, 1146–1148.

Kress, V.C., Carmichael, I.S.E., 1991. The compressibility of silicate liquids containing Fe_2O_3 and the effect of composition, temperature, oxygen fugacity and pressure on their redox states. Contributions to Mineralogy and Petrology 108, 82–92.

Lange, R., Carmichael, I., 1990. Thermodynamic properties of silicate liquids with emphasis on density, thermal expansion and compressibility. In: Nicholls, J., Russell, J. (Eds.), Modern Methods of Igneous Petrology, Mineralogical Society of America, Reviews in Mineralogy, vol. 24, pp. 25–64.

Lattard, D., Sauerzapf, U., Käsemann, M., 2005. New calibration data for the Fe–Ti oxide thermo-oxybarometers from experiments in

the Fe–Ti–O system at 1 bar, 1,000–1,300 °C and a large range of oxygen fugacities. Contributions to Mineralogy and Petrology 149 (6), 735–754.

Lindsley, D.H., 2003. Do Fe–Ti oxide magmas exist? Geology: Yes; Experiments: No! Norges Geologiske Undersøkelse Special Publication, vol. 9, pp. 34–35.

McBirney, A.R., 1995. Mechanisms of differentiation of the Skaergaard intrusion. Journal of the Geological Society of London 152, 421–435.

Morse, S.A., 1982. A partisan review of Proterozoic anorthosites. American Mineralogist 67 (11–12), 1087–1100.

Morse, S.A., 1996. Kiglapait mineralogy III: olivine compositions and Rayleigh fractionation models. Journal of Petrology 37 (5), 1037–1061.

Philpotts, A.R., 1967. Origin of certain iron–titanium oxide and apatite rocks. Economic Geology 62, 303–315.

Rivers, T., Martignole, J., Gower, C.F., Davidson, A., 1989. New tectonic divisions of the Grenville Province, southeastern Canadian Shield. Tectonics 8, 63–84.

Roelandts, I., Duchesne, J.C., 1979. Rare-earth elements in apatite from layered norites and iron–titanium oxide ore-bodies related to anorthosites (Rogaland, S.W. Norway). In: Ahrens, L.H. (Ed.), Origin and distribution of the elements. Pergamon Press, Oxford, New York, pp. 199–212.

Scoates, J.S., 2000. The plagioclase-magma density paradox re-examined and the crystallization of Proterozoic anorthosites. Journal of Petrology 41, 627–649.

Snyder, D., Carmichael, I.S.E., Wiebe, R.A., 1993. Experimental study of liquid evolution in an Fe-rich, layered mafic intrusion: constraints of Fe–Ti oxide precipitation on the T-fO_2 and T-ρ paths of tholeiitic magmas. Contributions to Mineralogy and Petrology 113, 73–86.

Sun, S.-s., McDonough, W.F., 1989. Chemical and isotopic systematics of oceanic basalts: implication for mantle composition and process. In: Saunders, A.D., Norry, M.J. (Eds.), Magmatism in the Ocean Basins. Spec. Publ. Vol. Geol. Soc. Lond. , pp. 313–345.

Tollari, N., Toplis, M.J., Barnes, S.-J., 2006. Predicting phosphate saturation in silicate magmas: an experimental study of the effects of melt composition and temperature. Geochimica et Cosmochimica Acta 70 (6), 1518–1536.

Toplis, M.J., Carroll, M.R., 1995. An experimental study of the influence of oxygen fugacity on Fe–Ti oxide stability, phase relations, and mineral-melt equilibria in ferro-basaltic systems. Journal of Petrology 36 (5), 1137–1170.

Toplis, M.J., Corgne, A., 2002. An experimental study of element partitioning between magnetite, clinopyroxene and iron-bearing silicate liquids with particular emphasis on vanadium. Contributions to Mineralogy and Petrology 144 (1), 22–37.

Toplis, M.J., Dingwell, D., Libourel, G., 1994. The effect of phosphorous on the iron redox ratio, viscosity, and density of an evolved ferrobasalt. Contributions to Mineralogy and Petrology 117, 293–304.

van Breemen, O., Higgins, M.D., 1993. U–Pb zircon age of the southwest lobe of the Havre-Saint-Pierre Anorthosite Complex, Grenville Province, Canada. Canadial Journal of Earth Science 30, 1453–1457.

Vander Auwera, J., Longhi, J., 1994. Experimental study of a jotunite (hypersthene monzodiorite): constraints on the parent magma composition and crystallization conditions (P, T, f_{O2}) of the Bjerkreim–Sokndal layered intrusion (Norway). Contributions to Mineralogy and Petrology 118, 60–78.

Vander Auwera, J., Bologne, G., Roelandts, I., Duchesne, J.C., 1998a. Inductively coupled plasma-mass spectrometric (ICP-MS) analysis of silicate rocks and minerals. Geologica Belgica 1, 49–53.

Vander Auwera, J., Longhi, J., Duchesne, J.C., 1998b. A liquid line of descent of the jotunite (hypersthene monzodiorite) suite. Journal of Petrology 39, 439–468.

Vander Auwera, J., Weis, D., Duchesne, J.C., 2006. Marginal mafic intrusions as indicators of downslope draining of dense residual melts in anorthositic diapirs? Lithos 89 (3–4), 329–352.

Wager, L.R., Brown, G.M., 1968. Layered Igneous Rocks. Oliver & Boyd, Edinburgh. 588 pp.

Watson, T.L., Taber, S., 1910. Nelsonite, a new rock type; its occurrence, association, and composition. Geological Society of America Bulletin 21, 787.

Wiebe, R.A., Snyder, D., 1993. Slow, dense replenishments of a basic magma chamber: the layered series of the Newark Island layered intrusion, Nain, Labrador. Contributions to Mineralogy and Petrology 113, 59–72.

Wilson, J.R., Robins, B., Nielsen, F.M., Duchesne, J.C., Vander Auwera, J., 1996. The Bjerkreim–Sokndal layered intrusion, Southwest Norway. In: Cawthorn, R.G. (Ed.), Layered Intrusions. Elsevier, Amsterdam, pp. 231–255.

Wodicka, N., David, J., Parent, M., Gobeil, A., Verpaelst, P., 2003. Géochronologie U–Pb et Pb–Pb de la région de Sept-Îles—Natashquan, Province de Grenville, Moyenne-Côte-Nord. In: Brisebois, D., Clark, T. (Eds.), Géologie et Ressources Minérales de la Partie Est de la Province de Grenville. Ministère des Ressources naturelles de la Faune et des Parcs, Québec, DV 2002–03, pp. 59–117.